City Research Online

City, University of London Institutional Repository

This is the accepted version of the paper.

This version of the publication may differ from the final published version.

A spectral dynamic stiffness method for free vibration analysis of plane elastodynamic problems

X. Liu[*], J.R. Banerjee

School of Mathematics, Computer Sciences and Engineering, City, University of London, London EC1V 0HB, UK

Abstract

A highly efficient and accurate analytical spectral dynamic stiffness (SDS) method for modal analysis of plane elastodynamic problems based on both plane stress and plane strain assumptions is presented in this paper. First, the general solution satisfying the governing differential equation exactly is derived by applying two types of one-dimensional modified Fourier series. Then the SDS matrix for an element is formulated symbolically using the exact general solution. The SDS matrices are assembled directly in a similar way to that of the finite element method, demonstrating the method's capability to model complex structures. Any arbitrary boundary conditions are represented accurately in the form of the modified Fourier series. The Wittrick-Williams algorithm is then used as the solution technique where the mode count problem (J_0) of a fully-clamped element is resolved. The proposed method gives highly accurate solutions with remarkable computational efficiency, covering low, medium and high frequency ranges. The method is applied to both plane stress and plane strain problems with simple as well as complex geometries. All results from the theory in this paper are accurate up to the last figures quoted to serve as benchmarks.

Keywords: Spectral dynamic stiffness method (SDSM), plane stress vibration, plane strain vibration, modal analysis, modified Fourier series, Wittrick-Williams algorithm.

1. Introduction

A wide range of three-dimensional elastodynamic problems are generally treated by two-dimensional (plane) theories, which include plane stress and plane strain theories. The plane stress theory assumes that the stress perpendicular to the plane

---

[*]Corresponding author
Email address: `xiangliu06@gmail.com` (X. Liu)

under consideration is always zero. This is often the case for plates whose upper and bottom surfaces are free. The vibration of such a plate in its own plane is generally called inplane vibration. Despite the fact that the transverse vibration [1] is usually given more importance for plate-like structures which are more easily excited by transverse external forces rather than inplane forces, there are many instances when inplane vibration can have pronounce effects. As a consequence, there has been an increasing interest in the inplane vibration of plates and plate assemblies. For instance, inplane vibrations are very important for built-up structures [2] where two or more plates are connected at a certain angle such that the transverse and inplane vibrations are directly coupled. The inplane vibrations become even more important in the mid to high frequency ranges for noise control and energy transmission analyses of structures [3, 4]. Examples include the walls of aerospace structures, the hulls of ships and cutting tools. The plane strain theory on the other hand, is widely used to investigate the free vibration of engineering structures like earth dams [5], shear wall structures [6] and thin or thick hollow cylinders [7–10]. For example, the earth dams and shear wall structures are designed to counter the effect of lateral dynamic loads caused by earthquake or wind. The plane strain theory is also widely used in plane wave propagation problems [11], which have applications in non-destructive testing [12, 13] and phononic crystal analysis [14]. Some other investigators have used the plane strain theory to study the mechanism of edge effects on the natural vibration and wave propagation properties of thick multi-layered plates [15, 16]. As the natural mode shapes can be regarded as the standing waves of a structure with the prescribed boundary conditions, the plane strain free vibration can provide important information for wave propagation problems with respect to different boundary conditions or discontinuities.

Without doubt, the above problems can be solved by the finite element method (FEM) with many well-developed commercial packages which can handle complex geometries. However, the FEM may become inadequate and unreliable when modelling structures within medium to high frequency ranges. In order to capture the relatively short wavelengths of structural deformations in these frequencies, an FEM model may require prohibitively large number of degrees of freedom (DOF) and even then the results can be still unreliable. Furthermore, for optimisation and parametric studies, the FEM becomes less attractive because of the considerable computational cost and/or the requirement of remeshing the structures. Therefore, analytical methods that are both efficient and accurate should be developed, which will facilitate efficient parametric and optimisation studies by varying significant parameters.

There are a few exact or analytical methods for plane elastodynamic problems, but even so, these methods are generally limited to simple geometries and restricted boundary conditions. It is well known that the closed-form exact solu-

2

tion for free inplane vibration (plane stress) is available only for rectangular plates with a pair of opposite edges simply supported. The earliest research on this topic was probably conducted by Lord Rayleigh [17]. Much later, Gorman [18] carried out a thorough investigation for exact solutions of simply supported plates by using Levy-type solutions. Xing and Liu [19–21] provided closed-form exact solutions for all possible cases of simply supported plates by using the Rayleigh quotient method. The classical dynamic stiffness method [22–25], first developed for plates in the 70s [22], can be applied to plate assemblies but restricted to cases with two opposite plate edges simply supported. Plates with other boundary conditions are solved resorting to other analytical methods. Bardell et al. [23] used the Rayleigh-Ritz method to discuss the free inplane vibration of single plates with simply supported, fully clamped and completely free boundary conditions. Dozio [26] used the Ritz method in conjunction with a set of trigonometric functions to study the free inplane vibration of plates with elastic boundaries. Farag and Pan [27, 28] made use of two types of series solution in the forced response analysis to examine the inplane vibration of rectangular plates with a pair of opposite edges clamped and other two edges being either clamped or free. The same cases were solved by Wang and Wereley [29], utilising the Kantorovich variational method. Gorman employed a systematic superposition method to study the free inplane vibration of completely free [30] and fully clamped [18] plates. Nefovska-Danilovic et al [31] developed the dynamic stiffness method for isotropic rectangular plates based on Gorman's superposition method. Du et al. [32, 33] used a Fourier series based analytical method to examine the free inplane vibration of plates with different boundary conditions. More recently, Papkov [34] provided the lower and upper bounds of natural frequencies for the free inplane vibration of completely free and fully clamped plates by an analytical method which makes use of the asymptotic behaviour of quasi-regular infinite systems. There is much less work on the free vibration of 3D solid structures under plane strain deformation. Such analysis is generally based on numerical methods. Tsiatas and Gazetas [5] applied an FEM model for plane-strain free vibration of earth dams. Nardini and Brebbia [6] developed a boundary element method for plane strain vibrations. There are even less papers on analytical methods for plane strain vibration. Gazis [7] derived the exact solution for the plane-strain vibration of a thick hollow cylinder. Ahmed [8] used a generalised Fourier-series technique for the axisymmetric plane-strain vibrations of a thick-layered orthotropic cylinder. Dong et al [15, 16] made use of a direct-iterative eigensolution technique to investigate the edge effects in laminated plates. However, most of the above analytical methods are limited to single rectangular or annular domain and thus can not be applied to complex geometries.

There is a recently developed analytical method called the SDS method (SDSM [35–37], by the authors) which can handle complex geometries with any arbitrary boundary conditions. This method has been developed for the biharmonic

3

equation [35–37] which governs the transverse vibration of thin plates. The formulated SDS matrices can be assembled directly to allow the modelling of complex geometries just like the FEM, but importantly the adopted shape function in the SDS method (SDSM) is exact instead of approximate as in the FEM. Therefore highly accurate solutions can be obtained from the SDSM by using as few elements as possible. Besides, the SDS formulation represents infinite degrees of freedom (DOF) accurately and efficiently by using only a very few DOF along the structure boundaries. As a results, the proposed method can provide highly accurate natural frequencies and modal shapes with remarkable computational efficiency, which is much superior to both the conventional FEM and BEM, not only within low frequency range, but also within medium to high frequency ranges. Furthermore, the SDSM has the certainty that no natural frequency of the structure will be missed and no spurious modes will be captured. The above superiorities of SDSM plus its analytical essence provide a huge advantage for parametric studies and structural optimisation.

The main purpose of this paper is to generalised the previous SDSM for biharmonic equation [35–37] to Navier's equation governing plane elastodynamic problems covering both plane stress and plane strain assumptions. However, the SDSM development for plane elastodynamic problems in the current research is different and indeed a formidable challenge compared to that in the biharmonic equation for thin plates [35–37]. This is due to the fact that previous investigations [35–37] involved only one variable as opposed to two variables encountered here. Moreover, there is a 90° phase differences between the expressions for the two variables and between the associated boundary conditions in the plane elastodynamic problems. All of the above differences increase the complexity many folds, given the fact that completely arbitrary BCs will be accounted for and analytical instead of numerical formulations are to be developed. Therefore, the earlier SDS formulation through the solution of the biharmonic equation [35–37] as well as the associated building blocks (e.g., the J_0 count) need to be generalised in the new SDSM development for plane elastodynamic problems. More importantly, the differential equation governing plane elastodynamic problems represents a model for a wide range of other partial differential equations (PDEs) and therefore the generalised SDS formulation in this paper will no-doubt establish a more general framework for the SDS formulation for other PDEs, e.g., different versions of Helmholtz equations and Maxwell equation. It should be noted that the proposed method can also be applied to wave propagation (dynamic response) analysis, but this paper focuses only on modal analysis. It is well known that the modal analysis of structures within low frequency range is a fundamental prerequisite for elastodynamic analysis, not only to avoid resonance but also for further dynamic response and aeroelastic analyses; the modal analysis within medium to high frequency ranges is important, for instance, to evaluate the structures' acous-

4

tic performance as well as energy flow properties.

This paper is organised as follows. After this introduction section, the governing differential equation (GDE) and general boundary conditions (BC) are derived by using Hamilton's principle through a coordinate-free tensor form in Section 2.1. Section 2.2 presents the attainment of exact general solution using two types of modified Fourier series. Then the spectral dynamic stiffness (SDS) matrix for an individual element is formulated through symbolic manipulation; the element SDS matrices can be assembled to form a global SDS matrix to model complex geometries subject to any arbitrary boundary conditions, see Section 2.4. In Section 2.5, the Wittrick-William algorithm is applied and the so-called J_0 count problem is resolved. Convergence, accuracy and computational efficiency studies are presented in Section 3.1. The theory of this paper is applied to both plane stress (Section 3.2) and plane strain (Section 3.3) problems for benchmark cases as well as engineering applications. Finally, the principal conclusions of this work are reported in Section 4.

2. Theory

2.1. Governing differential equation and general boundary conditions

The governing differential equation (GDE) and the corresponding natural boundary conditions (BCs) for plane elastodynamic problems are derived using Hamilton's principle. The application of the Hamilton's principle will not only lead to the GDE but also relate the generalised forces and displacements BCs which facilitate the spectral dynamic stiffness (SDS) formulation in the next step. The GDE and BCs are derived in a coordinate-free tensorial form which is applicable to both plane stress and plane strain vibration problems.

Assuming that a three-dimensional (3D) elastic body undergoing vibration described by the contravariant basis $\mathcal{B} = \{\boldsymbol{g}_1, \boldsymbol{g}_2, \boldsymbol{g}_3\}$ with $\boldsymbol{g}_3 \cdot \boldsymbol{g}_1 = \boldsymbol{g}_3 \cdot \boldsymbol{g}_2 = 0$, the geometry, material properties, deformation and boundary conditions of the 3D body may then be considered not to vary in the $\boldsymbol{g}_3$ direction. Therefore, the deformation of the 3D body can be represented by the deformation of the cross section occupying Ω bounded by $\partial\Omega$. Hamilton's principle for the cross section Ω can then be written in the usual notation as

$$\delta \int_{t_1}^{t_2} (\mathcal{K} - \mathcal{W} + \mathcal{W}_e)\mathrm{d}t = 0 \,, \tag{1}$$

where $\mathcal{K}$ and $\mathcal{W}$ are respectively the kinetic and elastic energies of the body on the cross section Ω, and $\mathcal{W}_e$ is the work done by external loads $\boldsymbol{q}$ on the boundary $\partial\Omega$ (assuming no body force is applied) so that

$$\mathcal{K} = \frac{1}{2}\int_\Omega \rho\dot{\boldsymbol{u}} \cdot \dot{\boldsymbol{u}}\mathrm{d}A \,, \quad \mathcal{W} = \frac{1}{2}\int_\Omega \boldsymbol{\sigma} : \boldsymbol{e}\mathrm{d}A \,, \quad \mathcal{W}_e = \int_{\partial\Omega} \boldsymbol{q} \cdot \boldsymbol{u}\mathrm{d}s \,, \tag{2}$$

5

where ρ is the density of the elastic body; $\dot{(\ )}$ denotes the derivative of $(\ )$ with respect to time; $\boldsymbol{e}$ and $\boldsymbol{\sigma}$ are linear strain and Cauchy stress tensors respectively with

$$\boldsymbol{e} = \frac{1}{2}(\boldsymbol{u} \otimes \boldsymbol{\nabla} + \boldsymbol{\nabla} \otimes \boldsymbol{u}) := (\boldsymbol{\nabla} \otimes \boldsymbol{u})^s \tag{3}$$

and

$$\boldsymbol{\sigma} = \lambda \mathrm{tr}(\boldsymbol{e})\boldsymbol{I} + 2\mu\boldsymbol{e} = \lambda(\boldsymbol{\nabla} \cdot \boldsymbol{u})\boldsymbol{I} + 2\mu(\boldsymbol{\nabla} \otimes \boldsymbol{u})^s \tag{4}$$

and where λ and μ are the *effective* Lamé constants of the cross section made of a certain isotropic material. Here, λ takes different expressions for plane stress (λ^e) and plane strain (λ^a) deformation in terms of engineering elastic constants E and ν; whereas μ (which is essentially the shear modulus G) takes a unique expression, namely

$$\lambda = \begin{cases} \lambda^e = \dfrac{E\nu}{1 - \nu^2} & \text{plane stress} \\ \lambda^a = \dfrac{E\nu}{(1 + \nu)(1 - 2\nu)} & \text{plane strain} \end{cases}, \quad \mu = G = \frac{E}{2(1 + \nu)}. \tag{5}$$

It should be mentioned in passing that λ^e or λ^a can be obtained by letting $\sigma^{33} = 0$ or $e^{33} = 0$, respectively when reducing the Hooke's law from a 3D problem into a 2D (plane) problem. A close inspection on the Eq. (5) reveals that $\lambda^a > \lambda^e$ for $\nu \in [0, 0.5)$. It is therefore expected that the natural frequencies for the plane strain deformation will be always larger than those under plane stress deformation when all other factors are identical. Also, it is easily seem that λ^a is the same as that of 3D solid whereas λ^e is somehow different.

After routine manipulations, Eq. (1) leads to

$$\delta \int_{t_1}^{t_2} \left[\int_\Omega (\boldsymbol{\nabla} \cdot \boldsymbol{\sigma} - \rho\ddot{\boldsymbol{u}}) \cdot \delta\boldsymbol{u}\,\mathrm{d}A + \int_{\partial\Omega} (\boldsymbol{q} - \boldsymbol{\sigma} \cdot \boldsymbol{n}) \cdot \delta\boldsymbol{u}\,\mathrm{d}s \right] \mathrm{d}t = 0. \tag{6}$$

In view of Eq. (4) and due to the complete arbitrariness of $\delta\boldsymbol{u}$, the first terms in the square brackets on the left hand side of Eq. (6) leads to the GDE in the form

$$\boldsymbol{\nabla} \cdot \boldsymbol{\sigma} - \rho\ddot{\boldsymbol{u}} = (\lambda + \mu)\boldsymbol{\nabla}(\boldsymbol{\nabla} \cdot \boldsymbol{u}) + \mu\nabla^2\boldsymbol{u} - \rho\ddot{\boldsymbol{u}} = \boldsymbol{0}, \tag{7}$$

which is the so-called Navier's equation. Now introducing the local coordinates $\{\boldsymbol{n}, \boldsymbol{s}\}$ attached to the boundary $\partial\Omega$ where $\boldsymbol{n}$ and $\boldsymbol{s}$ are normal and tangent unit vectors forming an orthonormal basis, the second term in the square brackets on the left hand side of Eq. (6) becomes

$$\int_{\partial\Omega} (\boldsymbol{q} - \boldsymbol{\sigma} \cdot \boldsymbol{n}) \cdot \delta\boldsymbol{u}\,\mathrm{d}s = \int_{\partial\Omega} (\boldsymbol{q} - \boldsymbol{\sigma} \cdot \boldsymbol{n}) \cdot (\delta u_n\boldsymbol{n} + \delta u_s\boldsymbol{s})\,\mathrm{d}s = 0 \tag{8}$$
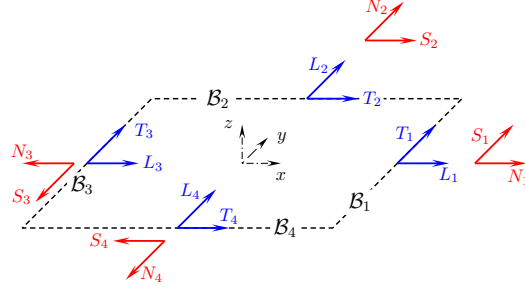
Figure 1: Coordinate system and notations for a rectangular element.

By substituting Eq. (4) into Eq. (8), the natural BCs can now be written in the form

$$\delta u_n: \; q_n = \boldsymbol{\sigma} \cdot \boldsymbol{n} \cdot \boldsymbol{n} = \lambda \boldsymbol{\nabla} \cdot \boldsymbol{u} + 2\mu \nabla_n u_n = (\lambda + 2\mu)\nabla_n u_n + \lambda \nabla_s u_s \,, \quad (9a)$$

$$\delta u_s: \; q_s = \boldsymbol{\sigma} \cdot \boldsymbol{n} \cdot \boldsymbol{s} = \mu(\nabla_n u_s + \nabla_s u_n) \,, \quad (9b)$$

where $q_n = \boldsymbol{q} \cdot \boldsymbol{n}$ and $q_s = \boldsymbol{q} \cdot \boldsymbol{s}$.

We will first aim to obtain the spectral dynamic stiffness (SDS) matrix of a rectangular element for the plane elastodynamic problems, see Fig. 1, following which, complex geometries will be modelled as an assembly of SDS elements. If Cartesian coordinate system (x, y) is introduced with the origin placed at the centre of the rectangular, so that $(x, y) \in [-a, a] \times [-b, b] = \Omega$ for $\boldsymbol{u} = [u, v]^T$, the GDE of Eq. (7) becomes

$$(\lambda + 2\mu)u_{,xx} + \mu u_{,yy} + (\lambda + \mu)v_{,xy} - \rho \ddot{u} = 0 \,, \quad (10a)$$

$$(\lambda + 2\mu)v_{,yy} + \mu v_{,xx} + (\lambda + \mu)u_{,xy} - \rho \ddot{v} = 0 \,, \quad (10b)$$

where the suffix after the comma denotes the corresponding partial derivatives. If harmonic oscillation is assumed $\boldsymbol{u} = \boldsymbol{U} \exp(-i\omega t)$ where $\boldsymbol{U} = [U, V]^T$, the GDE in the frequency domain can be derived from Eq. (10) to give

$$a_1 U_{,xx} + U_{,yy} + a_2 V_{,xy} + \kappa U = 0 \,, \quad (11a)$$

$$a_1 V_{,yy} + V_{,xx} + a_2 U_{,xy} + \kappa V = 0 \,, \quad (11b)$$

where

$$a_1 = a_0 + 2 \,, \; a_2 = a_0 + 1 \,, \; a_0 = \lambda/\mu \,, \; \kappa = \rho \omega^2 / G \,. \quad (12)$$

By recalling Eq. (5), a_0 (and therefore a_1 and a_2) will have different expressions for plane stress and plane stress deformation, namely,

$$a_0 = \begin{cases} a_0^e = \dfrac{2\nu}{1 - \nu} & \text{plane stress} \\[2mm] a_0^a = \dfrac{2\nu}{1 - 2\nu} & \text{plane strain} \end{cases} . \quad (13)$$

7

The natural BCs in the frequency domain along the four boundaries $\mathcal{B}_i$ (i=1,2,3,4) of the rectangular element in Fig. 1 are obtained by applying Eq. (9) to the four boundaries to give

$$\delta L_i : \ N_i \,, \quad \delta T_i : \ S_i \,, \qquad i = 1, 2, 3, 4 \,, \tag{14}$$

where the direction of L_i, N_i, T_i and S_i are given in Fig. 1 with the following expressions

$$\begin{bmatrix} L_1 \\ T_1 \\ L_2 \\ T_2 \\ L_3 \\ T_3 \\ L_4 \\ T_4 \end{bmatrix} = \begin{bmatrix} U|_{x=a} \\ V|_{x=a} \\ V|_{y=b} \\ U|_{y=b} \\ U|_{x=-a} \\ V|_{x=-a} \\ V|_{y=-b} \\ U|_{y=-b} \end{bmatrix} \,, \quad \begin{bmatrix} N_1 \\ S_1 \\ N_2 \\ S_2 \\ N_3 \\ S_3 \\ N_4 \\ S_4 \end{bmatrix} = G \begin{bmatrix} (a_1 U_{,x} + a_0 V_{,y})|_{x=a} \\ (U_{,y} + V_{,x})|_{x=a} \\ (a_1 V_{,y} + a_0 U_{,x})|_{y=b} \\ (U_{,y} + V_{,x})|_{y=b} \\ -(a_1 U_{,x} + a_0 V_{,y})|_{x=-a} \\ -(U_{,y} + V_{,x})|_{x=-a} \\ -(a_1 V_{,y} + a_0 U_{,x})|_{y=-b} \\ -(U_{,y} + V_{,x})|_{y=-b} \end{bmatrix} \,. \tag{15}$$

Here, L_i and T_i are introduced to denote the normal u_n and tangent u_s displacements of Eq. (9) respectively along the ith boundary $\mathcal{B}_i$ whereas N_i and S_i are the longitudinal (q_n) and shear (q_s) forces along the same boundaries. It is worth emphasising that $L_i(N_i)$ and $T_i(S_i)$ are defined either by $U(\sigma_{xx})$ and $V(\sigma_{xy})$ or by $V(\sigma_{yy})$ and $U(\sigma_{xy})$, depending on the corresponding boundaries. For plane stress vibration which consists of elements of different thicknesses h, the coefficient G in Eq. (15) will be replaced by Gh to incorporate the contribution of thickness in each element.

Next, the exact general solution of Eq. (11) will be derived which provides complete flexibility to describe any arbitrary BCs of Eq. (15).

2.2. Spectral representation of exact general solution and general boundary conditions

One of the most challenging problems in the SDSM development is the derivation of the exact general solution of GDE subject to any arbitrary BCs, which is without doubt more challenging than the classical dynamic stiffness method (DSM) development under simply support assumptions. This is because the SDSM is for a real two-dimensional (2D) problem whereas the classical DSM is somehow for a quasi-one-dimensional (1D) problem (either for beam elements or for Levy-type plate elements with a pair of opposite edges simply supported).

As mentioned in the Introduction, the SDS formulation for plane elastodynamic problems is expected to be very different from that developed earlier for the biharmonic equation governing flexural free vibration of thin plates [35–37]. This is because there are two functions $U(x, y)$ and $V(x, y)$ involved in the GDE

8

(11) rather than only one $W(x, y)$ encountered earlier in the biharmonic equation. Besides, there is a $90°$ phase difference between U and V in the GDE (11) as well as between $L_i(N_i)$ and $T_i(S_i)$ in the BCs, see Eq. (15).

Accordingly, in the current SDSM development for plane elastodynamic problems, two (rather than only one [35–37]) types of modified Fourier basis functions (MFBF) and the corresponding modified Fourier series (MFS) need to be introduced. They are given in Section 2.2.1. These two types of MFBF and MFS are adopted not only to obtain the exact general solution of the GDE (Section 2.2.2) but also to transform any arbitrary BCs into the corresponding coefficient vectors, see Section 2.2.3.

2.2.1. Modified Fourier basis functions and the corresponding modified Fourier series

Two types of MFBF and the corresponding MFS are presented in this section, both of which will be used in the SDSM development later in this paper. The first MFBF is the one that was already utilised in the SDSM development for biharmonic equation [35–37], namely

$$\mathcal{T}_l(\gamma_{ls}\xi) = \begin{cases} \cos(\gamma_{ls}\xi) & l = 0 \\ \sin(\gamma_{ls}\xi) & l = 1 \end{cases}, \quad \gamma_{ls} = (s + \frac{l}{2})\frac{\pi}{L}, \tag{16}$$

where $\xi \in [-L, L]$, $s \in \mathbb{N} = \{0, 1, 2, \dots\}$. The expressions in Eq. (16) are essentially the eigenfunctions of 1D Laplace operator equipped with *zero Neumann* BCs. This set of MFBF has been proved mathematically [38] to form a complete orthogonal set. The corresponding MFS exhibits a much fast convergence rate (asymptotic order two) than the classical Fourier series (asymptotic order one only) when representing analytic, non-periodic functions, see [39]. Indeed, the corresponding MFS is a powerful and elegant tool which partly contributes to the remarkable accuracy and numerical stability of the previous SDSM in [35–37].

However, in the current SDSM formulation for plane elastodynamic problems, apart from the above MFBF given by Eq. (16), another type of MFBF is also required, namely,

$$\mathcal{T}_l^*(\gamma_{ls}\xi) = \begin{cases} \sin(\gamma_{ls}\xi) & l = 0 \\ \cos(\gamma_{ls}\xi) & l = 1 \end{cases}. \tag{17}$$

The expressions of Eq. (17) are essentially the eigenfunctions of the Laplace operator equipped with *zero Dirichlet* BCs. The notations l, s, ξ, γ_{ls} are the same as those in Eq. (16). It is apparent that the two MFBF correspond to the first derivatives of each other with respect to ξ. Therefore, the two MFBF of Eqs. (16) and (17) form a *conjugate* pair. The above conjugate property is a crucial factor which will be used in the current SDSM development to cope with the $90°$ phase

different between U and V and between the BCs. The first few terms of the two types of MFBF are illustrated in Appendix A.

There are different adaptations of modified Fourier series (MFS) corresponding to the MFBF described above in Eqs. (16) and (17). In the current SDSM, the following two sets of MFS related to MFBF defined in Eqs. (16) and (17) are proposed. For any 1D arbitrary function $h(\xi), \xi \in [-L, L]$ subjected to *Dirichlet-type BC* (with arbitrary Dirichlet BC, i.e., $h(\pm L)$, but with zero Neumann BC, i.e., $d_\xi h(\pm L) = 0$), one can write

$$h(\xi) = \sum_{\substack{s \in \mathbb{N} \\ l \in \{0,1\}}} H_{ls} \frac{\mathcal{T}_l(\gamma_{ls}\xi)}{\sqrt{\zeta_{ls}L}} \,, \ H_{ls} = \int_{-L}^{L} h(\xi) \frac{\mathcal{T}_l(\gamma_{ls}\xi)}{\sqrt{\zeta_{ls}L}} \mathrm{d}\xi \,, \tag{18}$$

where

$$\zeta_{ls} = \begin{cases} 2 & l = 0 \text{ and } s = 0 \\ 1 & l = 1 \text{ or } s \geq 1 \end{cases} \,. \tag{19}$$

For any 1D arbitrary function $h(\xi), \xi \in [-L, L]$ subjected to *Neumann-type BC* (with arbitrary Neumann BC, i.e., $d_\xi h(\pm L)$, but with zero Dirichlet BC, i.e., $h(\pm L) = 0$), one can write

$$h(\xi) = \sum_{\substack{s \in \mathbb{N} \\ l \in \{0,1\}}} H_{ls} \frac{\mathcal{T}_l^*(\gamma_{ls}\xi)}{\sqrt{\zeta_{ls}L}} \,, \ H_{ls} = \int_{-L}^{L} h(\xi) \frac{\mathcal{T}_l^*(\gamma_{ls}\xi)}{\sqrt{\zeta_{ls}L}} \mathrm{d}\xi \,. \tag{20}$$

Similar to [35], $\sqrt{\zeta_{ls}L}$ is introduced in Eqs. (18) and (20) to eliminate the dependence on the length of the integral range $[-L, L]$ and to retain the symplecticity [40] in the formulated SDSM.

Next, the above two sets of MFBF given by Eqs. (16) and (17) will be applied to derive the exact general solution of the GDE of Eq. (11) and the corresponding two types of MFS in Eqs. (18) and (20) will be used to transform the general BCs given by Eq. (15).

2.2.2. Spectral representation of exact general solution

The exact general solutions for both $U(x, y)$ and $V(x, y)$ of Eq. (11) can be appropriately expressed by the combination of two series with the aid of the two type of MFBF given by Eqs. (16) and (17) as follows

$$U(x, y) = \sum_{\substack{m \in \mathbb{N} \\ k \in \{0,1\}}} \mathcal{T}_k^*(\alpha_{km}x)U_{km}(y) + \sum_{\substack{n \in \mathbb{N} \\ j \in \{0,1\}}} U_{jn}(x)\mathcal{T}_j(\beta_{jn}y) \,, \tag{21a}$$

$$V(x, y) = \sum_{\substack{m \in \mathbb{N} \\ k \in \{0,1\}}} \mathcal{T}_k(\alpha_{km}x)V_{km}(y) + \sum_{\substack{n \in \mathbb{N} \\ j \in \{0,1\}}} V_{jn}(x)\mathcal{T}_j^*(\beta_{jn}y) \,, \tag{21b}$$

10

where $\mathcal{T}_k, \mathcal{T}_j$ and $\mathcal{T}_k^*, \mathcal{T}_j^*$ are MFBF defined in Eqs. (16) and (17) respectively with the wavenumbers $\alpha_{km} = (m + k/2)\pi/a$ and $\beta_{jn} = (n + j/2)\pi/b$; $U_{km}(y)$, $U_{jn}(x)$, $V_{km}(y)$ and $V_{jn}(x)$ are 1D functions to be determined exactly from the GDE in the next step. It should be noted here that both $U(x,y)$ and $V(x,y)$ are expressed by the combination of two series: the first series is expanded using the MFBF in x with the corresponding y-components exactly derived from the GDE; the second one is expanded using the MFBF in y with the corresponding x-components exactly derived. The combination of such two series instead of only one is essential to establish a complete solution space for both $U(x,y)$ and $V(x,y)$ governed by the GDE of Eq. (11). Another point needs to be emphasised is that the second series of $U(x,y)$ and the first series of $V(x,y)$ in Eq. (21) are expressed in terms of MFBF of Eq. (16) whereas the first series of $U(x,y)$ and the second series of $V(x,y)$ are expressed in terms of the MFBF of Eq. (17). This is because $U(x,y)$ and $V(x,y)$ denote the deformations in x and y directions respectively and therefore, have a 90° phase difference. It will become more transparent in the later formulation that Eq. (21) is indeed the unique expansion which guarantees that the k and j subscripts will correspond correctly to the symmetric and antisymmetric properties of the related mode shapes.

Now we are in position to derive the unknown functions $U_{km}(y), U_{jn}(x), V_{km}(y)$ and $V_{jn}(x)$ of Eq. (21). Substituting Eq. (21) into GDE of Eq. (10) and collecting similar terms of the MFBF yeild the following two ordinary differential equations (ODE) sets

$$\begin{bmatrix} d_y^2 + \kappa - a_1\alpha_{km}^2 & -\mu_1 d_y \\ \mu_1 d_y & a_1 d_y^2 + \kappa - \alpha_{km}^2 \end{bmatrix} \begin{bmatrix} U_{km}(y) \\ V_{km}(y) \end{bmatrix} = \begin{bmatrix} 0 \\ 0 \end{bmatrix} \; (\forall)k \in \{0,1\}, m \in \mathbb{N} \text{ except } k = m = 0 \quad (22a)$$

$$\begin{bmatrix} a_1 d_x^2 + \kappa - \beta_{jn}^2 & \mu_2 d_x \\ -\mu_2 d_x & d_x^2 + \kappa - a_1\beta_{jn}^2 \end{bmatrix} \begin{bmatrix} U_{jn}(x) \\ V_{jn}(x) \end{bmatrix} = \begin{bmatrix} 0 \\ 0 \end{bmatrix} \; (\forall)j \in \{0,1\}, n \in \mathbb{N} \text{ except } j = n = 0 \quad (22b)$$

where $d_x^i = d^i/dx^i$, $d_y^i = d^i/dy^i$ and $\mu_1 = (-1)^k a_2\alpha_{km}, \mu_2 = (-1)^j a_2\beta_{jn}$. (The two special cases when $k = m = 0$ and $j = n = 0$ will be treated at the end of this section.) Notice that Eqs. (22a) and (22b) are simultaneous ODE with constant coefficients, therefore it is appropriate to assume that $U_{km}(y) = \delta_{km}V_{km}(y)$ with $V_{km}(y) = \exp(t_{km}y)$ and $V_{jn}(x) = \delta_{jn}U_{jn}(x)$ with $U_{jn}(x) = \exp(r_{jn}x)$. Consequently, the characteristic equations of Eqs. (22a) and (22b) are respectively given by

$$a_1 t_{km}^4 + b_2 t_{km}^2 + c_2 = 0 \qquad (23a)$$
$$a_1 r_{jn}^4 + b_1 r_{jn}^2 + c_1 = 0 \qquad (23b)$$

where

$$b_2 = (a_1 + 1)\kappa - 2a_1\alpha_{km}^2 \qquad c_2 = (\kappa - \alpha_{km}^2)(\kappa - a_1\alpha_{km}^2),$$
$$b_1 = (a_1 + 1)\kappa - 2a_1\beta_{jn}^2, \qquad c_1 = (\kappa - \beta_{jn}^2)(\kappa - a_1\beta_{jn}^2).$$

11

It is easily seen that Eq. (23a) has four roots $\pm t_{1km}$ and $\pm t_{2km}$ and Eq. (23b) also has four roots $\pm r_{1jn}$ and $\pm r_{2jn}$, where

$$\left.\begin{array}{c} t_{1km} \\ t_{2km} \end{array}\right\} = \sqrt{\frac{-b_2 \mp \sqrt{b_2^2 - 4a_1 c_2}}{2a_1}}, \quad \left.\begin{array}{c} r_{1jn} \\ r_{2jn} \end{array}\right\} = \sqrt{\frac{-b_1 \mp \sqrt{b_1^2 - 4a_1 c_1}}{2a_1}}. \tag{24}$$

Thus the general solutions for $U_{km}(y), V_{km}(y), U_{jn}(x)$ and $V_{jn}(x)$ in Eqs. (21) are

$$\begin{cases} U_{km}(y) = \delta_{1km}\tilde{C}_{1km}\text{ch}(t_{1km}y) + \delta_{1km}\tilde{C}_{2km}\text{sh}(t_{1km}y) + \delta_{2km}\tilde{C}_{3km}\text{ch}(t_{2km}y) + \delta_{2km}\tilde{C}_{4km}\text{sh}(t_{2km}y) \\ V_{km}(y) = \tilde{C}_{1km}\text{ch}(t_{1km}y) + \tilde{C}_{2km}\text{sh}(t_{1km}y) + \tilde{C}_{3km}\text{ch}(t_{2km}y) + \tilde{C}_{4km}\text{sh}(t_{2km}y) \end{cases}$$
$$\tag{25a}$$

$$\begin{cases} U_{jn}(x) = \tilde{D}_{1jn}\text{ch}(r_{1jn}x) + \tilde{D}_{2jn}\text{sh}(r_{1jn}x) + \tilde{D}_{3jn}\text{ch}(r_{2jn}x) + \tilde{D}_{4jn}\text{sh}(r_{2jn}x) \\ V_{jn}(x) = \delta_{1jn}\tilde{D}_{1jn}\text{ch}(r_{1jn}x) + \delta_{1jn}\tilde{D}_{2jn}\text{sh}(r_{1jn}x) + \delta_{2jn}\tilde{D}_{3jn}\text{ch}(r_{2jn}x) + \delta_{2jn}\tilde{D}_{4jn}\text{sh}(r_{2jn}x) \end{cases}$$
$$\tag{25b}$$

where δ_{ikm} and δ_{ijn} $(i = 1, 2)$ are obtained by inserting Eqs. (25) into Eqs. (22) to give

$$\delta_{ikm} = -\frac{a_1 t_{ikm}^2 + \kappa - \alpha_{km}^2}{\mu_1 t_{ikm}}, \quad \delta_{ijn} = -\frac{a_1 r_{ijn}^2 + \kappa - \beta_{jn}^2}{\mu_2 r_{ijn}}. \tag{26}$$

Also, the following identities can be obtained based on Eqs. (22)

$$(a_1 r_{ijn}^2 + \kappa - \beta_{jn}^2)(r_{ijn}^2 + \kappa - a_1 \beta_{jn}^2) + \mu_2^2 r_{ijn}^2 = 0, \tag{27a}$$

$$(t_{ikm}^2 + \kappa - a_1 \alpha_{km}^2)(a_1 t_{ikm}^2 + \kappa - \alpha_{km}^2) + \mu_1^2 t_{ikm}^2 = 0. \tag{27b}$$

In what follows, the exact general solution obtained above will be partitioned into four symmetric/antisymmetric components. This will be taken advantage of in the subsequent SDSM development leading to analytical expressions by using the two types of MFBF discussed earlier. This procedure will also contribute to the reduction of the computation cost. Thus $U(x, y)$ and $V(x, y)$ given by Eqs (21) and (25) can be decomposed into four kj components

$$U(x, y) = \sum_{k,j \in \{0,1\}} U^{kj}(x, y) = U^{00} + U^{01} + U^{10} + U^{11}, \tag{28a}$$

$$V(x, y) = \sum_{k,j \in \{0,1\}} V^{kj}(x, y) = V^{00} + V^{01} + V^{10} + V^{11}, \tag{28b}$$

where k or j taking 0 and 1 denotes symmetric and antisymmetric deformation, respectively. However, the partition in the present work for the plane elastodynamic problems requires more special attention when compared to that in the transverse vibration problems [35–37]. It is very important to determine the appropriate symmetric or antisymmetric properties of U^{kj} and V^{kj}. The most appropriate way is to determine their symmetric/antisymmetric properties based on the longitudinal deformation. Therefore, U^{0j} and V^{1j} are antisymmetric in x whereas U^{1j} and V^{0j} are symmetric in x $(j \in \{0, 1\})$; U^{k0} and V^{k1} are symmetric in y whereas U^{k1} and

V^{k0} are antisymmetric in y ($k \in \{0, 1\}$). In this way, U^{kj} and V^{kj} can be represented by considering the appropriate symmetric/antisymmetric properties of the MFBF and the hyperbolic functions

$$U^{kj}(x,y) = \sum_{m\in\mathbb{N}} \left[\mathcal{T}_k^*(\alpha_{km}x) \sum_{i=1,2} (\delta_{ikm}C_{ikm}\mathcal{H}_j(t_{ikm}y)) \right] + \sum_{n\in\mathbb{N}} \left[\sum_{i=1,2} (D_{ijn}\mathcal{H}_k^*(r_{ijn}x)) \mathcal{T}_j(\beta_{jn}y) \right],$$
(29a)

$$V^{kj}(x,y) = \sum_{m\in\mathbb{N}} \left[\mathcal{T}_k(\alpha_{km}x) \sum_{i=1,2} (C_{ikm}\mathcal{H}_j^*(t_{ikm}y)) \right] + \sum_{n\in\mathbb{N}} \left[\sum_{i=1,2} (\delta_{ijn}D_{ijn}\mathcal{H}_k(r_{ijn}x)) \mathcal{T}_j^*(\beta_{jn}y) \right],$$
(29b)

where C_{ikm} and D_{ijn} are unknowns to be determined, and $\mathcal{H}_k, \mathcal{H}_j$ and $\mathcal{H}_k^*, \mathcal{H}_j^*$ stand for hyperbolic functions defined as follows.

$$\mathcal{H}_j(t_{ikm}y) = \begin{cases} \mathrm{ch}(t_{ikm}y) & j=0 \\ \mathrm{sh}(t_{ikm}y) & j=1 \end{cases}, \quad \mathcal{H}_k(r_{ijn}x) = \begin{cases} \mathrm{ch}(r_{ijn}x) & k=0 \\ \mathrm{sh}(r_{ijn}x) & k=1 \end{cases}, \quad (30a)$$

$$\mathcal{H}_j^*(t_{ikm}y) = \begin{cases} \mathrm{sh}(t_{ikm}y) & j=0 \\ \mathrm{ch}(t_{ikm}y) & j=1 \end{cases}, \quad \mathcal{H}_k^*(r_{ijn}x) = \begin{cases} \mathrm{sh}(r_{ijn}x) & k=0 \\ \mathrm{ch}(r_{ijn}x) & k=1 \end{cases}. \quad (30b)$$

Attention should be drawn to the above deduction from Eqs. (22) to (29) for two special cases. When $k = m = 0$ and $j = n = 0$, Eqs. (22a) and (22b) will reduce to second-order equations both of which will lead to two roots $\pm t_{00}$ and $\pm r_{00}$ with

$$t_{00} = r_{00} = \sqrt{-\kappa/a_1}. \tag{31}$$

Accordingly, Eq. (25) becomes

$$U_{km} = 0, \quad V_{km} = \tilde{C}_{100}\mathrm{ch}(t_{00}y) + \tilde{C}_{200}\mathrm{sh}(t_{00}y), \quad \text{when } k = m = 0, \quad (32a)$$

$$V_{jn} = 0, \quad U_{jn} = \tilde{D}_{100}\mathrm{ch}(r_{00}x) + \tilde{D}_{200}\mathrm{sh}(r_{00}x), \quad \text{when } j = n = 0. \quad (32b)$$

As a result, when $j = n = 0$, the zero term ($n = 0$) of the second series in Eq. (29a) becomes $D_{00}\mathcal{H}_0^*(r_{00}x)$; when $k = m = 0$, the zero term ($m = 0$) of the first series in Eq. (29b) becomes $C_{00}\mathcal{H}_0^*(t_{00}y)$.

2.2.3. Spectral representation of general boundary conditions

Due to the 90° phase difference between L_i (N_i) and T_i (S_i), the two types of MFS of Eqs. (16) and (17) are adopted to transform any arbitrarily prescribed BCs L_i, N_i and T_i, S_i respectively on the ith boundary $\mathcal{B}_i$. To this end, one has the corresponding modified Fourier coefficient vectors

$$\boldsymbol{f} = \left[\boldsymbol{N}_1^T, \boldsymbol{S}_1^T, \boldsymbol{N}_2^T, \boldsymbol{S}_2^T, \boldsymbol{N}_3^T, \boldsymbol{S}_3^T, \boldsymbol{N}_4^T, \boldsymbol{S}_4^T\right]^T, \tag{33a}$$

$$\boldsymbol{d} = \left[\boldsymbol{L}_1^T, \boldsymbol{T}_1^T, \boldsymbol{L}_2^T, \boldsymbol{T}_2^T, \boldsymbol{L}_3^T, \boldsymbol{T}_3^T, \boldsymbol{L}_4^T, \boldsymbol{T}_4^T\right]^T, \tag{33b}$$

13

where

$$\boldsymbol{N}_i = [N_{i00}, N_{i01}, \cdots, N_{i0s}, \cdots, N_{i10}, N_{i11}, \cdots, N_{i1s}, \cdots]^T, \tag{34a}$$

$$\boldsymbol{S}_i = [S_{i01}, \cdots, S_{i0s}, \cdots, S_{i10}, S_{i11}, \cdots, S_{i1s}, \cdots]^T, \tag{34b}$$

$$\boldsymbol{L}_i = [L_{i00}, L_{i01}, \cdots, L_{i0s}, \cdots, L_{i10}, L_{i11}, \cdots, L_{i1s}, \cdots]^T, \tag{34c}$$

$$\boldsymbol{T}_i = [T_{i01}, \cdots, T_{i0s}, \cdots, T_{i10}, T_{i11}, \cdots, T_{i1s}, \cdots]^T. \tag{34d}$$

Here, the sub-vectors $\boldsymbol{N}_i$ and $\boldsymbol{L}_i$ are the modified Fourier coefficient vectors of the BCs on $\mathcal{B}_i$ of the element by applying the MFS (16) to N_i and L_i of Eq. (15) respectively, and $\boldsymbol{S}_i$ and $\boldsymbol{T}_i$ are the corresponding modified Fourier coefficient vectors by applying the MFS (17) to S_i and T_i of Eq. (15) respectively. For example,

$$N_{ils} = \int_{-L}^{L} \frac{N_i}{G} \frac{\mathcal{T}_l(\gamma_{ls}\xi)}{\sqrt{\zeta_{ls}L}} \mathrm{d}\xi, \quad T_{ils} = \int_{-L}^{L} T_i \frac{\mathcal{T}_l^*(\gamma_{ls}\xi)}{\sqrt{\zeta_{ls}L}} \mathrm{d}\xi,$$

where $l \in \{0, 1\}, s \in \mathbb{N}$, ξ denotes either x or y and $2L$ is the boundary length representing either $2a$ or $2b$ in this paper. It should be noted that S_{i00} and T_{i00} are zero because $\mathcal{T}_0^*(\gamma_{00}\xi) \equiv 0$ based on Eq. (17). Therefore, both S_{i00} and T_{i00} have been deleted from the vectors $\boldsymbol{S}_i$ and $\boldsymbol{T}_i$ respectively to avoid null rows or columns.

2.3. Development of the spectral dynamic stiffness matrix of an element

The general solution obtained in Section 2.2.2 will serve as the exact shape function to develop the spectral dynamic stiffness (SDS) matrix for an element in this section. The analytical formulation procedure for the plane vibration in this paper is similar to but different from that for the transverse vibration [35]. First, the formulation for the four component SDS matrices $\boldsymbol{K}^{kj}$ is provided in Section 2.3.1. Then, the four component matrices $\boldsymbol{K}^{kj}$ will be combined in a suitable way to form the complete SDS matrix $\boldsymbol{K}$ for the whole element, see Section 2.3.2.

2.3.1. Development of the SDS component matrix $\boldsymbol{K}^{kj}$

Essentially, the component SDS matrix $\boldsymbol{K}^{kj}$ relates the generalised displacement and force BCs

$$[L_a^{kj}, L_b^{kj}, T_a^{kj}, T_b^{kj}]^T, [N_a^{kj}, N_b^{kj}, S_a^{kj}, S_b^{kj}]^T, \tag{35}$$

both of which are caused by the deformation described by the kj component of general solution, namely, U^{kj} and V^{kj}. In short, the formulation of the component SDS matrices $\boldsymbol{K}^{kj}$ is accomplished by substituting U^{kj} and V^{kj} into the generalised displacement and force BCs and eliminating the unknowns in U^{kj} and V^{kj}.

This includes two steps. Firstly, all unknown coefficients $C_{00}, C_{1km}, C_{2km}, D_{00}, D_{1jn}$ and D_{2jn} in the solution component of Eq. (29) are determined through the procedure described in Appendix C, which is essentially based on the expressions of $L_a^{kj}, L_b^{kj}, S_a^{kj}$ and S_b^{kj} in Eq. (C.1). (Compared to the transverse vibration formulation [35], special attention should be paid here in the determination for D_{00} (when $n = j = 0$) and C_{00} (when $k = m = 0$). Subsequently, an infinite system of algebraic equations is derived by substituting the above determined unknowns into the remaining entries $T_a^{kj}, T_b^{kj}, N_a^{kj}$ and N_b^{kj} in Eq. (C.1) and applying the modified Fourier series formula (A.1) to the hyperbolic functions, see Appendix D for details. This infinite system can be rewritten in the following mixed-variable matrix form as:

$$\begin{bmatrix} \boldsymbol{T}^{kj} \\ \boldsymbol{N}^{kj} \end{bmatrix} = \begin{bmatrix} \boldsymbol{A}_{TL}^{kj} & \boldsymbol{A}_{TS}^{kj} \\ \boldsymbol{A}_{NL}^{kj} & \boldsymbol{A}_{NS}^{kj} \end{bmatrix} \begin{bmatrix} \boldsymbol{L}^{kj} \\ \boldsymbol{S}^{kj} \end{bmatrix} . \tag{36}$$

The explicit expressions of the four coefficient matrices $\boldsymbol{A}_{\bullet\bullet}^{kj}$ in Eq. (36) are given in Appendix E, which are concise and easy to be implemented in programming. The sub-vectors of Eq. (36) are defined as

$$\boldsymbol{T}^{kj} = [T_{aj0}, T_{aj1}, \cdots, T_{ajn}, \cdots, T_{bk0}, T_{bk1}, \cdots, T_{bkm}, \cdots]^T , \tag{37a}$$

$$\boldsymbol{N}^{kj} = [N_{aj0}, N_{aj1}, \cdots, N_{ajn}, \cdots, N_{bk0}, N_{bk1}, \cdots, N_{bkm}, \cdots]^T , \tag{37b}$$

$$\boldsymbol{L}^{kj} = [L_{aj0}, L_{aj1}, \cdots, L_{ajn}, \cdots, L_{bk0}, L_{bk1}, \cdots, L_{bkm}, \cdots]^T , \tag{37c}$$

$$\boldsymbol{S}^{kj} = [S_{aj0}, S_{aj1}, \cdots, S_{ajn}, \cdots, S_{bk0}, S_{bk1}, \cdots, S_{bkm}, \cdots]^T \tag{37d}$$

whose entries are the Fourier coefficients in Eq. (C.1). Each entry of the above vectors corresponds to a frequency-wavenumber dependent DOF. It should be noted that when $k = m = 0$ or $j = n = 0$, the term S_{a00}, S_{b00} and T_{a00}, T_{b00} in Eqs. (37d) and (37a) are zero and should be removed from the matrices $\boldsymbol{S}^{kj}$ and $\boldsymbol{T}^{kj}$ respectively. Also, the mixed formulation of Eq. (36) facilitates resolving the so-called J_0 count problem which will be described later in Section 2.5.

On the basis of Eq. (36), the SDS matrix for each kj component can be reconstructed in the following form

$$\boldsymbol{f}^{kj} = \boldsymbol{K}^{kj} \boldsymbol{d}^{kj} , \tag{38}$$

in which

$$\boldsymbol{f}^{kj} = G \begin{bmatrix} \boldsymbol{N}^{kj} \\ \boldsymbol{S}^{kj} \end{bmatrix} , \quad \boldsymbol{d}^{kj} = \begin{bmatrix} \boldsymbol{L}^{kj} \\ \boldsymbol{T}^{kj} \end{bmatrix} , \tag{39}$$

$$\boldsymbol{K}^{kj} = G \begin{bmatrix} \boldsymbol{A}_{NL}^{kj} - \boldsymbol{A}_{NS}^{kj} \boldsymbol{A}_{TS}^{kj}{}^{-1} \boldsymbol{A}_{TL}^{kj} & \boldsymbol{A}_{NS}^{kj} \boldsymbol{A}_{TS}^{kj}{}^{-1} \\ \boldsymbol{A}_{TS}^{kj}{}^{-1} \boldsymbol{A}_{TL}^{kj} & \boldsymbol{A}_{TS}^{kj}{}^{-1} \end{bmatrix} . \tag{40}$$

15

(Note that the structure of the $\boldsymbol{K}^{kj}$ above takes different form compared to that in the transverse vibration formulation, i.e., Eq. (29) in [35].) In Eq. (40), G is the shear rigidity defined in Eq. (5) which results from Eq. (C.1b). As mentioned earlier at the end of Section 2.1, G will be replaced by Gh in plane stress problems to consider the contribution of different thickness of each element.

2.3.2. Integration of component SDS matrices to the elemental SDS matrix

The integration of component SDS matrices to the elemental SDS matrix is similar to that for the transverse vibration [35]. Therefore, $\boldsymbol{f}, \boldsymbol{d}$ of Eq. (33) can be related to $\boldsymbol{f}^{kj}, \boldsymbol{d}^{kj}$ of Eq. (39) in the form

$$\boldsymbol{f} = \boldsymbol{T}[\boldsymbol{f}^{00T}, \boldsymbol{f}^{01T}, \boldsymbol{f}^{10T}, \boldsymbol{f}^{11T}]^T, \quad [\boldsymbol{d}^{00T}, \boldsymbol{d}^{01T}, \boldsymbol{d}^{10T}, \boldsymbol{d}^{11T}]^T = \frac{1}{2}\boldsymbol{T}^T\boldsymbol{d}. \quad (41)$$

However, in Eq. (41), the transfer matrix $\boldsymbol{T}$ is determined by the relationships of Eqs. (B.2) and (B.3) of Appendix B, which takes the different form compared to that in the transverse vibration formulation in [35], namely

$$\boldsymbol{T} = \begin{bmatrix}
\boldsymbol{I}_n & \boldsymbol{O} & \boldsymbol{O} & \boldsymbol{O} & \boldsymbol{O} & \boldsymbol{O} & \boldsymbol{O} & \boldsymbol{O} & \boldsymbol{I}_n & \boldsymbol{O} & \boldsymbol{O} & \boldsymbol{O} & \boldsymbol{O} & \boldsymbol{O} & \boldsymbol{O} & \boldsymbol{O} \\
\boldsymbol{O} & \boldsymbol{O} & \boldsymbol{O} & \boldsymbol{O} & \boldsymbol{I}_n & \boldsymbol{O} & \boldsymbol{O} & \boldsymbol{O} & \boldsymbol{O} & \boldsymbol{O} & \boldsymbol{O} & \boldsymbol{O} & \boldsymbol{I}_n & \boldsymbol{O} & \boldsymbol{O} & \boldsymbol{O} \\
\boldsymbol{O} & \boldsymbol{O} & \boldsymbol{I}_n^\dagger & \boldsymbol{O} & \boldsymbol{O} & \boldsymbol{O} & \boldsymbol{O} & \boldsymbol{O} & \boldsymbol{O} & \boldsymbol{O} & \boldsymbol{I}_n^\dagger & \boldsymbol{O} & \boldsymbol{O} & \boldsymbol{O} & \boldsymbol{O} & \boldsymbol{O} \\
\boldsymbol{O} & \boldsymbol{O} & \boldsymbol{O} & \boldsymbol{O} & \boldsymbol{O} & \boldsymbol{O} & \boldsymbol{I}_n & \boldsymbol{O} & \boldsymbol{O} & \boldsymbol{O} & \boldsymbol{O} & \boldsymbol{O} & \boldsymbol{O} & \boldsymbol{O} & \boldsymbol{I}_n & \boldsymbol{O} \\
\boldsymbol{O} & \boldsymbol{I}_m & \boldsymbol{O} & \boldsymbol{O} & \boldsymbol{O} & \boldsymbol{I}_m & \boldsymbol{O} & \boldsymbol{O} & \boldsymbol{O} & \boldsymbol{O} & \boldsymbol{O} & \boldsymbol{O} & \boldsymbol{O} & \boldsymbol{O} & \boldsymbol{O} & \boldsymbol{O} \\
\boldsymbol{O} & \boldsymbol{O} & \boldsymbol{O} & \boldsymbol{O} & \boldsymbol{O} & \boldsymbol{O} & \boldsymbol{O} & \boldsymbol{O} & \boldsymbol{O} & \boldsymbol{I}_m & \boldsymbol{O} & \boldsymbol{O} & \boldsymbol{O} & \boldsymbol{I}_m & \boldsymbol{O} & \boldsymbol{O} \\
\boldsymbol{O} & \boldsymbol{O} & \boldsymbol{O} & \boldsymbol{I}_m^\dagger & \boldsymbol{O} & \boldsymbol{O} & \boldsymbol{O} & \boldsymbol{I}_m^\dagger & \boldsymbol{O} & \boldsymbol{O} & \boldsymbol{O} & \boldsymbol{O} & \boldsymbol{O} & \boldsymbol{O} & \boldsymbol{O} & \boldsymbol{O} \\
\boldsymbol{O} & \boldsymbol{O} & \boldsymbol{O} & \boldsymbol{O} & \boldsymbol{O} & \boldsymbol{O} & \boldsymbol{O} & \boldsymbol{O} & \boldsymbol{O} & \boldsymbol{O} & \boldsymbol{I}_m & \boldsymbol{O} & \boldsymbol{O} & \boldsymbol{O} & \boldsymbol{I}_m \\
-\boldsymbol{I}_n & \boldsymbol{O} & \boldsymbol{O} & \boldsymbol{O} & \boldsymbol{O} & \boldsymbol{O} & \boldsymbol{O} & \boldsymbol{O} & \boldsymbol{I}_n & \boldsymbol{O} & \boldsymbol{O} & \boldsymbol{O} & \boldsymbol{O} & \boldsymbol{O} & \boldsymbol{O} & \boldsymbol{O} \\
\boldsymbol{O} & \boldsymbol{O} & \boldsymbol{O} & \boldsymbol{O} & -\boldsymbol{I}_n & \boldsymbol{O} & \boldsymbol{O} & \boldsymbol{O} & \boldsymbol{O} & \boldsymbol{O} & \boldsymbol{O} & \boldsymbol{O} & \boldsymbol{I}_n & \boldsymbol{O} & \boldsymbol{O} & \boldsymbol{O} \\
\boldsymbol{O} & \boldsymbol{O} & \boldsymbol{I}_n^\dagger & \boldsymbol{O} & \boldsymbol{O} & \boldsymbol{O} & \boldsymbol{O} & \boldsymbol{O} & \boldsymbol{O} & \boldsymbol{O} & -\boldsymbol{I}_n^\dagger & \boldsymbol{O} & \boldsymbol{O} & \boldsymbol{O} & \boldsymbol{O} & \boldsymbol{O} \\
\boldsymbol{O} & \boldsymbol{O} & \boldsymbol{O} & \boldsymbol{O} & \boldsymbol{O} & \boldsymbol{O} & \boldsymbol{I}_n & \boldsymbol{O} & \boldsymbol{O} & \boldsymbol{O} & \boldsymbol{O} & \boldsymbol{O} & \boldsymbol{O} & \boldsymbol{O} & -\boldsymbol{I}_n & \boldsymbol{O} \\
\boldsymbol{O} & -\boldsymbol{I}_m & \boldsymbol{O} & \boldsymbol{O} & \boldsymbol{O} & \boldsymbol{I}_m & \boldsymbol{O} & \boldsymbol{O} & \boldsymbol{O} & \boldsymbol{O} & \boldsymbol{O} & \boldsymbol{O} & \boldsymbol{O} & \boldsymbol{O} & \boldsymbol{O} & \boldsymbol{O} \\
\boldsymbol{O} & \boldsymbol{O} & \boldsymbol{O} & \boldsymbol{O} & \boldsymbol{O} & \boldsymbol{O} & \boldsymbol{O} & \boldsymbol{O} & \boldsymbol{O} & -\boldsymbol{I}_m & \boldsymbol{O} & \boldsymbol{O} & \boldsymbol{I}_m & \boldsymbol{O} & \boldsymbol{O} \\
\boldsymbol{O} & \boldsymbol{O} & \boldsymbol{O} & \boldsymbol{I}_m^\dagger & \boldsymbol{O} & \boldsymbol{O} & \boldsymbol{O} & -\boldsymbol{I}_m^\dagger & \boldsymbol{O} & \boldsymbol{O} & \boldsymbol{O} & \boldsymbol{O} & \boldsymbol{O} & \boldsymbol{O} & \boldsymbol{O} & \boldsymbol{O} \\
\boldsymbol{O} & \boldsymbol{O} & \boldsymbol{O} & \boldsymbol{O} & \boldsymbol{O} & \boldsymbol{O} & \boldsymbol{O} & \boldsymbol{O} & \boldsymbol{O} & \boldsymbol{O} & \boldsymbol{I}_m & \boldsymbol{O} & \boldsymbol{O} & \boldsymbol{O} & -\boldsymbol{I}_m
\end{bmatrix}, \quad (42)$$

where $\boldsymbol{I}_n, \boldsymbol{I}_n^\dagger, \boldsymbol{I}_m$ and $\boldsymbol{I}_m^\dagger$ are identity matrices of dimension $n, n-1, m$ and $m-1$ respectively, and $\boldsymbol{O}$ represents null matrices. Finally, putting Eqs. (38), (33) and (41) together yields the SDS matrix for the entire element as

$$\boldsymbol{f} = \boldsymbol{K}\boldsymbol{d}, \quad (43)$$

16

where

$$
\boldsymbol{K} = \frac{1}{2} \boldsymbol{T} \begin{bmatrix} \boldsymbol{K}^{00} & \boldsymbol{O} & \boldsymbol{O} & \boldsymbol{O} \\ \boldsymbol{O} & \boldsymbol{K}^{01} & \boldsymbol{O} & \boldsymbol{O} \\ \boldsymbol{O} & \boldsymbol{O} & \boldsymbol{K}^{10} & \boldsymbol{O} \\ \boldsymbol{O} & \boldsymbol{O} & \boldsymbol{O} & \boldsymbol{K}^{11} \end{bmatrix} \boldsymbol{T}^{T} \tag{44}
$$

is the SDS matrix of the entire element.

2.4. Assembly procedure and the application of any arbitrary boundary conditions

One of the major advantages of the current SDSM over other analytical methods lies in the fact that the SDS elements can be assembled to allow the modelling of complex geometries. The assembly procedure from the elemental SDS matrices $\boldsymbol{K}$ to form the final SDS matrix $\boldsymbol{K}_f$ is similar to that of the finite element method (FEM). The only exception is that SDS elements are connected by line nodes whereas the FEM elements are connected by point nodes. The assembly procedure has been described in [36] and will not be repeated here.

The other advantage of the current SDSM over other analytical or numerical methods is that in the SDSM any arbitrary boundary conditions (BCs) can be applied very easily and accurately in the strong form. These BCs can be arbitrarily prescribed ranging from classical, uniform elastic BCs or arbitrary non-uniformly distributed elastic supports, mass attachments as well as elastic coupling constraints [41]. For plane elastodynamic problems governed by Eq. (11), there are four types of classical BCs. For each ith boundary $\mathcal{B}_i$, one has the following four possible classical BCs

Clamped (C):	$L_i = T_i = 0$,	(45a)
Simply supported 1 (S$_1$):	$T_i = N_i = 0$,	(45b)
Simply supported 2 (S$_2$):	$L_i = S_i = 0$,	(45c)
Free (F):	$N_i = S_i = 0$.	(45d)

The final SDS matrix $\boldsymbol{K}_f$ of the whole structure can be condensed directly for the DOF fixed with zero displacement. More specifically, the rows and columns $\boldsymbol{K}_f$ which related to $\boldsymbol{L}_i$ and $\boldsymbol{T}_i$ will be condensed for 'C' boundaries; those related to $\boldsymbol{T}_i$ will be condensed for 'S$_1$' edges; those related to $\boldsymbol{L}_i$ will be condensed for 'S$_2$' edges; and of course, no condensation is required for 'F' edges.

2.5. The Wittrick-Williams algorithm enhancement and mode shape computation

In essence, the elegance of the SDSM lies in representing a dynamical system accurately by using an extremely small number of DOF in an analytical and concise manner. This makes the SDSM superior to other numerical or analytical methods in terms of both accuracy and computational efficiency within low,

medium and high frequency ranges. The merits of the SDSM are exploited by the application of the well-known Wittrick-Williams (WW) algorithm [42] which is further enhanced by some novel techniques as described in this section. Suppose that ω denotes the circular (or angular) frequency of a vibrating structure, then according to the WW algorithm, as ω is increased from zero to ω^*, the number of natural frequencies passed (J) is given by

$$J = J_0 + s\{\boldsymbol{K}_f\}, \tag{46}$$

where $s\{\boldsymbol{K}_f\}$ corresponds to the negative inertia of the final SDS matrix $\boldsymbol{K}_f$ evaluated at $\omega = \omega^*$; and J_0 is given by

$$J_0 = \sum_m J_{0m}, \tag{47}$$

where J_{0m} is the number of natural frequencies between $\omega = 0$ and $\omega = \omega^*$ for an individual component member when its boundaries are fully clamped. For more details, interested readers are referred to [35, 36, 42]. A similar strategy described in [35] is also adopted here to provide an efficient and reliable prediction for the above J_{0m} which is based on the closed-form solution of each members subject to full simple supports. Therefore, J_{0m} of Eq. (47) can be obtained by applying the WW algorithm in reverse to give

$$J_{0m} = J_{Sm} - s(\boldsymbol{K}_{Sm}), \tag{48}$$

where J_{Sm} is the overall mode count of a certain member with all boundaries subject to simple supports, and $s(\boldsymbol{K}_{Sm})$ is the sign count of its formulated SDS matrix $\boldsymbol{K}_{Sm}$. In the present method, the strategy based on Eq. (48) has been successfully implemented using the following steps.

First, the computation of J_{Sm} in Eq. (48) is accomplished in an analytical manner by solving a number theory problem. It is well-known that the exact solution for the natural frequency of an all-round simply supported (S_2) element is available [17, 19, 43]. The natural frequency $\omega_{\hat{m}\hat{n}}$ for the case can be expressed analytically in the following nondimensionalised form

$$\frac{2\rho}{G}\left(\frac{2a\omega_{\hat{m}\hat{n}}}{\pi}\right)^2 = a_1(\hat{m}^2 + \eta^2\hat{n}^2), \quad \hat{m}, \hat{n} \in \{1, 2, 3, ...\}, \tag{49}$$

and

$$\frac{2\rho}{G}\left(\frac{2a\omega_{\hat{m}\hat{n}}}{\pi}\right)^2 = (a_1 + 2)(\hat{m}^2 + \eta^2\hat{n}^2), \quad \hat{m}, \hat{n} \in \{0, 1, 2, 3, ...\} \text{ except } \hat{m} = \hat{n} = 0, \tag{50}$$
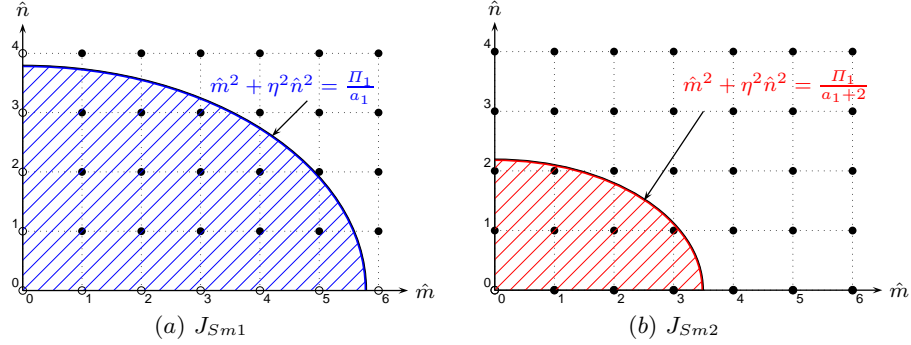
18

Figure 2: The mode counts J_{Sm1} and J_{Sm2} associated with Eqs. (49) and (50) are essentially extended Gauss circle problems illustrated in plots (a) and (b) respectively. Black solid dots are counted whereas empty circles are not counted. In both plots, $\Pi_1 = 2\rho \left(2a\omega^*/\pi\right)^2/G$.

where $\eta = a/b$ and $\hat{m}$ and $\hat{n}$ are the number of half-waves in the x and y direction respectively. Thus, J_{Sm}, the number of natural frequencies lying below a trial natural frequency ω^*, is essentially the total number of combinations of $(\hat{m}, \hat{n})$ such that the left-hand sides of Eqs. (49) and (50) with $\omega_{\hat{m}\hat{n}} = \omega^*$ are not smaller than the right-hand sides. Therefore,

$$J_{Sm} = J_{Sm1} + J_{Sm2}. \tag{51}$$

Obviously, J_{Sm1} and J_{Sm2} can be obtained from a numerical search which may be computationally expensive and the procedure may miss some of the natural frequencies. However, there exists an analytical expression for J_{Sm1} and J_{Sm1} and this problem is essentially an extension of the *Gauss circle problem* [44] in the field of number theory. In essence, J_{Sm1} is the number of black solid dots within the blue shaded region covered by the curve $\hat{m}^2 + \eta^2\hat{n}^2 = \Pi_1/a_1$ in Fig. 2(a); whereas J_{Sm2} is the number of black solid dots within the red shaded region covered by the curve $\hat{m}^2 + \eta^2\hat{n}^2 = \Pi_1/(a_1 + 2)$ in Fig. 2(b). The analytical expressions for J_{Sm1} and J_{Sm2} can be deduced by solving the inequalities for which the left-hand sides of Eqs. (49) and (50) with $\omega_{\hat{m}\hat{n}} = \omega^*$ are greater than the right-hand sides, hence

$$J_{Sm1} = \sum_{\hat{m}=1}^{\lfloor \Pi_2 \rfloor} \left\lfloor \sqrt{\frac{\Pi_1}{a_1} - \hat{m}^2}/\eta \right\rfloor, \quad J_{Sm2} = \sum_{\hat{m}=0}^{\lfloor \Pi_3 \rfloor} \left\lfloor \sqrt{\frac{\Pi_1}{a_1 + 2} - \hat{m}^2}/\eta + \text{sign}(\hat{m}) \right\rfloor, \tag{52}$$

where '$\lfloor \cdot \rfloor$' is the floor function denoting the largest integer not greater than '$\cdot$'

and

$$\varPi_1 = \left(\frac{2a}{\pi}\right)^2 \frac{2\rho\omega^{*2}}{G}\,,\ \varPi_2 = \sqrt{\frac{\varPi_1}{a_1} - \eta^2}\,,\ \varPi_2 = \sqrt{\frac{\varPi_1}{a_1 + 2} - \eta^2}\,.$$

Next, the computation of $s(\boldsymbol{K}_{Sm})$ in Eq. (48) is achieved in an elegant way by taking advantage of the mixed-variable formulation explained earlier in Section 2.3.1. Like in [35], when a rectangular element is subjected to all round simple supports as defined in Eq. (45c), the four symmetric/antisymmetric SDS matrices are decoupled. Hence, $s(\boldsymbol{K}_{Sm}) = \sum_{k,j\in\{0,1\}} s(\boldsymbol{K}_{Sm}^{kj})$. Now recalling Eqs. (38), (39) and (40), the case with fully simple supports of type S_2 becomes equivalent to letting $\boldsymbol{L}^{kj} = \boldsymbol{S}^{kj} = \boldsymbol{0}$, such that $s(\boldsymbol{K}_{Sm}^{kj}) = s(\boldsymbol{A}_{TS}^{kj\,-1})$. In this way, one has

$$s(\boldsymbol{K}_{Sm}) = \sum_{k,j\in\{0,1\}} s(\boldsymbol{A}_{TS}^{kj\,-1}) = \sum_{k,j\in\{0,1\}} s(\boldsymbol{A}_{TS}^{kj})\,, \tag{53}$$

which takes a simpler form than that for the transverse vibration [35] (Eq. 45 therein). The above technique of computing J_{Sm} and $s(\boldsymbol{K}_{Sm})$ resolves with conclusive certainty the problem of determining J_0 in a highly efficient, accurate and reliable manner. The mode shape computation follows similar procedure as in the SDSM for plate transverse vibration problem [36]. Therefore the details are not given here for conciseness (for more details please refer to [36]).

3. Results and applications

The SDSM described above is implemented in a `Matlab` program which gives highly accurate solutions for plane elastodynamic problems with remarkable computational efficiency. The convergence, accuracy and numerical efficiency studies are carried out in Section 3.1 below. Then the method is applied to both plane stress problems in Section 3.2 and plane strain problems in Section 3.3.

3.1. Convergence and efficiency investigations for low, medium and high frequency modes

Unlike most of other methods that are based on domain discretisation, there is no need to study the convergence of the current SDSM with respect to h-refinement. This is because the SDS formulation is based on exact general solution (shape function) and therefore, there is no need to discretise the analysis domain unless discontinuity of geometry or material properties exists. However, any arbitrarily prescribed boundary conditions along a certain line node (boundary) with infinite degrees of freedom (DOF) is represented accurately by the modified Fourier series. In the numerical implementation, those modified Fourier series should be truncated at a certain stage. Therefore, the convergence and numerical

Table 1: Convergence and efficiency studies for the dimensionless natural frequency parameter of a square isotropic plate ($\nu = 0.3$) with four sets of different BCs by using the SDSM. FEM solutions in comparison are obtained by (ANSYS) using a 300×300 mesh of Plane 182 elements (each element has four nodes with two DOFs at each node). The SDSM results for the $S_2S_1S_2S_1$ case are compared with exact solutions. Bold values are those for which the computed eignfrequencies using SDSM converge to the last figures of the presented values.

BC	$M = N$	$\lambda = 2\omega a/\pi\sqrt{\rho/G}$								Sig.Dig.	Time(s)
		1	2	3	4	5	6	7	8		
CCCC	2	1.91223	1.91223	2.27834	2.78883	3.15033	3.16444	3.16444	3.59928	4	0.09
	5	1.91282	1.91282	2.27861	2.79005	**3.15218**	3.17143	3.17143	3.60884	5	0.12
	10	**1.91284**	**1.91284**	**2.27861**	**2.79012**	**3.15218**	**3.17144**	**3.17144**	3.60899	6	0.12
	15	**1.91284**	**1.91284**	**2.27861**	**2.79012**	**3.15218**	**3.17144**	**3.17144**	3.60901	6	0.13
	20	**1.91284**	**1.91284**	**2.27861**	**2.79012**	**3.15218**	**3.17144**	**3.17144**	3.60901	6	0.13
	FEM	1.91287	1.91287	2.27863	2.79020	3.15229	3.17154	3.17154	3.60907	4	10.0
$S_2S_1S_2S_1$	2	**0.00000**	**1.00000**	**1.41421**	**1.69031**	**2.00000**	**2.23607**	**2.23607**	**2.39046**	6	0.32
	5	**0.00000**	**1.00000**	**1.41421**	**1.69031**	**2.00000**	**2.23607**	**2.23607**	**2.39046**	6	0.33
	10	**0.00000**	**1.00000**	**1.41421**	**1.69031**	**2.00000**	**2.23607**	**2.23607**	**2.39046**	6	0.38
	Exact	0.00000	1.00000	1.41421	1.69031	2.00000	2.23607	2.23607	2.39046	6	–
	FEM	0.00000	1.00001	1.41423	1.69031	2.00002	2.23614	2.23614	2.39048	5	10.0
CCCS$_2$	2	1.71589	1.89594	2.04652	2.61358	2.85040	3.02671	3.15582	3.47699	3	0.37
	5	1.71596	1.89625	2.04678	2.61394	2.85180	3.02733	3.15932	3.47827	4	0.40
	10	**1.71597**	**1.89626**	**2.04679**	**2.61396**	**2.85183**	**3.02734**	**3.15932**	**3.47830**	6	0.46
	15	**1.71597**	**1.89626**	**2.04679**	**2.61396**	**2.85183**	**3.02734**	**3.15932**	**3.47830**	6	0.54
	20	**1.71597**	**1.89626**	**2.04679**	**2.61396**	**2.85183**	**3.02734**	**3.15932**	**3.47830**	6	0.74
	FEM	1.71596	1.89628	2.04682	2.61400	2.85189	3.02745	3.15945	3.47840	4	10.0
CCS$_2$S$_2$	2	1.57608	1.80432	1.95874	2.34519	2.69515	2.84183	3.04571	3.43305	4	0.72
	5	**1.57609**	**1.80450**	**1.95877**	2.34533	**2.69570**	2.84248	**3.04628**	3.43397	5	0.76
	10	**1.57609**	**1.80450**	**1.95877**	2.34534	**2.69570**	2.84250	**3.04628**	3.43399	6	0.81
	15	**1.57609**	**1.80451**	**1.95877**	2.34534	**2.69570**	2.84250	**3.04628**	3.43399	6	1.04
	20	**1.57609**	**1.80451**	**1.95877**	2.34534	**2.69570**	2.84250	**3.04628**	3.43399	6	1.26
	FEM	1.57611	1.80451	1.95879	2.34539	2.69576	2.84258	3.04639	3.43407	5	11.0

efficiency investigations should be carried out. Table 1 shows four sets of results for the free inplane vibration of a square plate ($\nu = 0.3$) with different boundary conditions, namely, CCCC, $S_2S_1S_2S_1$, CCCS$_2$ and CCS$_2$S$_2$. Notice that in this paper, the letter C and F represent clamped and free edges respectively whereas S_1 and S_2 denote edges with two types of simple supports: S_1 edges having zero shear displacement and zero longitude forces (see Eq. (45b)) whilst S_2 having both longitude displacement and shear forces being zero, see Eq. (45b). The notation comprising four letters successively represent the right, up, left and bottom edges respectively in an anticlockwise sense. The first eight dimensionless natural frequencies $\lambda = 2\omega a/\pi\sqrt{\rho/G}$ are computed by the current SDSM using only one SDS element with different number of terms (M, N) adopted in the series, where $M = N$ and both vary from 2 to 20. The results are compared with finite element solutions computed by ANSYS using a very fine mesh with 300×300 Plane 182 elements. Among the four tabulated cases, closed-form exact solutions are available only for the $S_2S_1S_2S_1$ case which all coincide with the current SDSM results. The computation of both SDSM and FEM is performed on a PC equipped with a 3.4 GHz Intel 4-core processor and 8 GB of memory. The total execution time for the first eight natural frequencies is given in the last column of Table 1. It can be concluded that the SDSM converges very fast to exact solutions with respect to the terms adopted in the series. A five-term (ten-term) series gives accuracy with five (six) significant figures but the total computation time for these eight natural

frequencies is less than half a second. It can be seen from the table that the SDSM takes only 5% computation time of the well-developed commercial FEM package `ANSYS` which meanwhile, provides more accurate results that the FEM. Another important observation can be made is that the SDSM always gives exact results of the $S_2S_1S_2S_1$ irrespective of the number of terms adopted in the series. It is found that this is true for all cases with at least a pair of opposite edges are S_2 supported. The reason is due to the fact that the SDSM formulation is based on representing the unknowns of the general solution by $L_{ajn}, L_{bkm}, S_{ajn}$ and S_{bkm}, see Eqs. (C.5) and (C.6).

The remarkable accuracy and computational efficiency of the current SDSM is not only evident for low frequency range as shown above but also equally valid for medium to high frequency ranges. This is clear from Table 2 where the SDSM is used to predict the medium (10th-100th) and high (200th-1000th) natural frequencies for the same four cases studied earlier in Table 1. When using the SDSM, only one SDS element is used in the modelling with both M and N adopted as 20, and all SDSM results are given with accuracy of six significant figures. The results computed by SDSM are compared with FE solutions computed by `ANSYS` (using a 300×300 mesh of Plane 182 elements) with only three significant figures for the 10th-100th modes. Higher natural modes are not computed by the FEM since the solvers provided in the FEM becomes highly inefficient and unreliable for higher modes. The final matrix size and total computational time for both methods are also given in the last two rows of Table 2. To solve the tabulated 11 modes with six significant figures covering medium to high frequency ranges, the SDSM took only 0.25-1.25 s; whereas the well-developed FEM package `ANSYS` took 23-28 s but compute only the first six medium modes with three significant figures. It is apparent that SDSM is far more superior to the FEM in free vibration analysis within medium to high frequency ranges. The major advantage of the current SDSM lies in the fact that the SDS formulation satisfies the GDE exactly and uses extremely low number of DOF to represent the system most accurately. For the four case studies shown in Table 2, the final matrix size of the SDSM was only 39-158, which is in a sharp contrast to the FEM which used as many as 1.80E05 DOF. This great advantage establishes the SDSM as an ideal tool for parametric and optimisation studies, not only within low frequency range but also within medium to high frequency ranges.

3.2. Applications to plane stress problems

As mentioned earlier, the modal analysis of elastodynamic problems with plane stress assumption is essentially the free inplane vibration of plates. The current SDSM development allows us to carry out exact modal analysis of plate and plate assemblies subjected to any arbitrary boundary conditions.

22

Table 2: Numerical stability and efficiency studies of the SDSM using the same four cases given in Table 1. The same dimensionless natural frequency parameter as in Table 1 is used, i.e., $\lambda = 2\omega a/\pi\sqrt{\rho/G}$. The SDSM is applied to compute 11 natural frequencies of the four cases covering medium (10th-100th) to higher (200th-1000th) modes. Side by side are the finite element solutions obtained by `ANSYS` using a 300×300 mesh of Plane 182 elements, only medium (10th-100th) modes are given for the FE solutions. The final matrix size and the total computational time of both the SDSM and FEM are given in the last two rows.

Mode	CCCC		$S_2S_1S_2S_1$		$CCCS_2$		CCS_2S_2	
	SDSM	FEM	SDSM	FEM	SDSM	FEM	SDSM	FEM
10	**3.82718**	3.82859	**3**	3.00009	**3.72833**	3.72845	**3.56133**	3.56150
20	**5.17103**	5.17542	**4.12311**	4.12342	**5.07830**	5.07865	**4.93554**	4.93602
40	**6.91510**	6.92134	**6.08276**	6.08379	**6.80026**	6.80100	**6.59543**	6.59643
60	**8.38312**	8.38503	**7.28011**	7.28172	**8.22259**	8.22479	**8.01245**	8.01452
80	**9.36414**	9.36610	**8.60233**	8.60544	**9.31753**	9.31987	**9.22457**	9.22677
100	**10.5505**	10.5549	**9.84886**	9.85316	**10.3622**	10.3655	**10.1912**	10.1933
200	**14.5867**	–	**13.6277**	–	**14.4709**	–	**14.2358**	–
400	**20.2866**	–	**19.2725**	–	**20.1682**	–	**20.0177**	–
600	**24.5966**	–	**23.7697**	–	**24.4609**	–	**24.3223**	–
800	**28.2882**	–	**27.4591**	–	**28.1562**	–	**27.9424**	–
1000	**31.5344**	–	**30.6128**	–	**31.3854**	–	**31.2660**	–
Sign. Fig.	**6**	3	**6**	3	**6**	3	**6**	3
Matrix Size	**39**	1.80E+05	**158**	1.80E+05	**39**	1.80E+05	**78**	1.80E+05
Time (s)/modes	**0.25** /11	24.6 /6	**1.25** /11	23.5 /6	**1.06**/11	27.5 /6	**1.11**/11	23.0/6

The free inplane vibration analysis of plates has received much less attention compared to the out-of-plane free vibration analysis. There are only a few attempts in the literature using different methods which makes the current analysis even more important. As the first example, the current SDSM is applied to the free inplane vibration analysis of a fully clamped plate with different aspect ratios. Table 3 compares the first eight natural frequencies computed by the SDSM results with those obtained by other methods wherever available. The comparative methods include dynamic stiffness method based on the superposition method (DSM) [31], Gorman's superposition method (GSM) [18], Fourier series based analytical method (FSA) [32] and the Ritz method [23]. The current SDSM results, which are accurate up to the last figures quoted with six significant figures, are intended to serve as benchmark solutions. It can be found that the results computed by GSM [18] and Ritz method [23] have four significant figures which all coincide with the first four digits of the current SDSM results. The dynamic stiffness method based on the superposition method [31] appears to miss the repeated natural frequency for the square plate as denoted by '$**$' in Table 3. This might be due to the reason that determinant method rather than the WW algorithm was applied as the solution technique in this method [31]. (Although WW algorithm was mentioned briefly in the context of [31], it is apparent that the WW algorithm was after all not applied in its calculation, let alone how the important issue in the WW algorithm, the J_0 count, could be solved.) The first eight natural mode shapes for a fully clamped

square isotropic plate ($a/b = 1$) are plotted in Fig. 3 with the (k, j) notation given as follows: $(0, 0)$ modes are doubly symmetric about both x and y axes (Figs. 3(e) and (h)) whereas $(1, 1)$ modes are double antisymmetric modes (Figs. 3(c)), $(0, 1)$ modes are symmetric in x but antisymmetric in y (Figs. 3(a) and (f)) and $(1, 0)$ modes are antisymmetric in x but symmetric in y (Figs. 3(b) and (g)). It should be noted that the (k, j) notation here is different from the 'S'/'A' notation used by Gorman in [18]. As evident from Fig. 3, the (k, j) notation in this paper is more physically meaningful than that by Gorman [18] as the (k, j) in the current SDSM represents the actual symmetric or antisymmetric properties of the deformation. Moreover, it can be seen that the 1st and 2nd modes are longitudinally dominant whereas the 3rd mode is shear dominant. Other modes are somehow coupled modes of both longitudinal and shear deformation.

Table 3: The first eight dimensionless inplane natural frequencies of fully clamped isotropic rectangular plates with three different aspect ratios (a/b). The notations k (corresponding to x axis) and j (corresponding to y axis) of (k, j) denote symmetric (taking '0') or antisymmetric (taking '1') deformation with respect to the corresponding axes.

a/b	Method	$\lambda = 2\omega a\sqrt{\rho(1-\nu^2)/E}$							
		1	2	3	4	5	6	7	8
1	(k, j)	(0,1)	(1,0)	(1,1)	(1,1)	(0,0)	(0,1)	(1,0)	(0,0)
	SDSM	**3.55519**	**3.55519**	**4.23501**	**5.18570**	**5.85862**	**5.89441**	**5.89441**	**6.70768**
	DSM[a]	3.556	**	4.236	5.186	5.86	5.896	–	–
	GSM[b]	3.555	3.555	4.235	5.186	5.859	5.894	5.894	6.708
	FSA[c]	3.554	3.554	4.236	5.185	5.859	5.896	–	–
	Ritz[d]	3.555	3.555	4.235	5.186	5.859	5.895	–	–
2	(k, j)	(1,0)	(0,1)	(1,1)	(0,0)	(0,1)	(1,1)	(1,1)	(1,0)
	SDSM	**4.78902**	**6.37856**	**6.71212**	**7.04875**	**7.6083**	**8.14019**	**8.99796**	**9.51559**
	GSM[b]	4.789	6.379	6.712	7.049	7.608	8.140	8.998	9.515
	FSA[c]	4.788	6.374	6.710	7.048	7.608	8.140	–	–
	Ritz[d]	4.789	6.379	6.712	7.049	7.608	8.140	–	–
3	(k, j)	(1,0)	(0,0)	(0,1)	(1,1)	(0,1)	(1,0)	(1,1)	(1,1)
	SDSM	**6.33852**	**8.19699**	**9.39504**	**9.53980**	**10.0562**	**10.5429**	**10.7866**	**11.7899**
	FSA[c]	6.336	8.195	9.385	9.532	10.05	10.54	–	–

[a] Dynamic stiffness method based on the Gorman's superposition method [31]
[b] Gorman's superposition method [18]
[c] Fourier series based analytical method [32]
[d] Ritz method [23]

Similar comparison can be made for the free inplane vibration of completely free isotropic plates ($\nu = 0.3$) between the current SDSM results and those available in the literature [18, 23, 31, 32]. All SDSM results have six significant digit accuracy which are more accurate than those available in the literature (the latter methods give no more than three or four significant figures). It should be noted that the present SDSM is capable of capturing the first three zero frequencies corresponding to rigid modes due to the application of the WW algorithm. Ap-
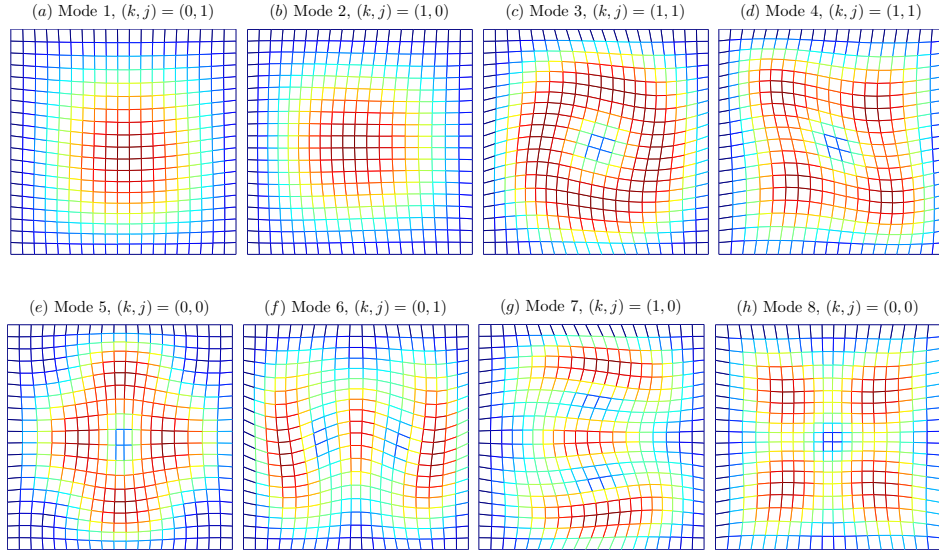
(a) Mode 1, $(k, j) = (0, 1)$ (b) Mode 2, $(k, j) = (1, 0)$ (c) Mode 3, $(k, j) = (1, 1)$ (d) Mode 4, $(k, j) = (1, 1)$

(e) Mode 5, $(k, j) = (0, 0)$ (f) Mode 6, $(k, j) = (0, 1)$ (g) Mode 7, $(k, j) = (1, 0)$ (h) Mode 8, $(k, j) = (0, 0)$

Figure 3: The first eight natural mode shapes of a fully clamped plate under free inplane vibration. The (k, j) notation was given in the caption of Table 3. The colour of the mesh, varying from blue to red, indicates the normalised displacement amplitude $\sqrt{U^2 + V^2}/\max(\sqrt{U^2 + V^2})$ varying from 0 to 1.

parently, these zero frequencies were missed by other investigators [18, 31, 32]. The first non-rigid body inplane mode shapes of a square isotropic plate is shown in Fig. 4 where (k, j) denotes the symmetric and antisymmetric properties of the deformation in a similar fashion to that of the previous fully clamped case.

Table 4: The first eight non-zero dimensionless inplane natural frequencies of completely free isotropic rectangular plates ($\nu = 0.3$) with three different aspect ratios a/b. The (k,j) notation is the same as that given in Table 3.

a/b	Methods	$\lambda = 2\omega a \sqrt{\rho(1-\nu^2)/E}$							
		4	5	6	7	8	9	10	11
1	(k,j)	(1,1)	(0,1)	(1,0)	(0,0)	(0,0)	(0,0)	(0,1)	(1,0)
	SDSM	**2.32060**	**2.47162**	**2.47162**	**2.62845**	**2.98739**	**3.45224**	**3.72312**	**3.72312**
	DSM[a]	2.320	2.472	**	2.628	2.988	3.452	3.724	**
	GSM[b]	2.320	2.472	2.472	2.628	2.988	3.452	3.724	3.724
	FSA[c]	2.321	2.472	2.472	2.629	2.988	3.452	–	–
	Ritz[d]	2.321	2.472	2.472	2.628	2.987	3.452	–	–
2	(k,j)	(0,1)	(0,0)	(1,1)	(1,1)	(0,1)	(0,0)	(1,0)	(1,0)
	SDSM	**1.95365**	**2.96082**	**3.26705**	**4.72633**	**4.78411**	**5.20446**	**5.25689**	**5.36510**
	GSM[b]	1.956	2.960	3.268	4.726	4.784	5.208	5.258	5.370
	FSA[c]	1.954	2.961	3.268	4.725	4.785	5.205	–	–
	Ritz[d]	1.954	2.961	3.267	4.726	4.784	5.205	–	–
3	(k,j)	(0,1)	(0,0)	(1,1)	(0,1)	(1,1)	(1,0)	(0,1)	(1,1)
	SDSM	**1.57065**	**2.98313**	**3.22219**	**4.9479**	**5.75158**	**5.82971**	**7.08253**	**7.21869**
	FSA[c]	1.571	2.983	3.224	4.951	5.754	5.83	–	–

[a] Dynamic stiffness method based on Gorman's superposition method [31]
[b] Gorman's superposition method [18]
[c] Fourier series based analytical method [32]
[d] Ritz method [23]

Table 5: The first eight inplane natural frequencies (Hz) of a rectangular plate with three different boundary conditions.

BC	Method	Mode (Hz)							
		1	2	3	4	5	6	7	8
CCCC	**SDSM**	**2665.39**	**2905.29**	**3277.77**	**4050.14**	**4306.88**	**4429.41**	**4819.31**	**5347.91**
	Kant.[a]	2667	2909	3280	4089	4327	4437	–	–
	FRA[b]	2671	2914	3349	4198	4404	4607	4917	5329
	FRA[c]	2666	2906	3279	4052	4308	4431	4820	5350
	FEM[d]	2658	2898	3260	4024	4268	4404	4769	5300
FCCC	**SDSM**	**1803.97**	**2658.89**	**2802.09**	**3405.33**	**3492.23**	**3729.25**	**4366.8**	**4628.53**
	FSA[e]	1802	2657	2800	3402	3492	3730	–	–
	Kant.[a]	1811	2674	2845	3524	3504	3757	–	–
	FRA[b]	1892	2727	3026	3596	3624	3868	4704	4899
	FEM[d]	1803	2656	2794	3392	3479	3704	4339	4589
FCFC	**SDSM**	**1447.32**	**2515.25**	**2568.25**	**2642.62**	**3042.92**	**3074.86**	**3938.5**	**4217.24**
	FSA[e]	1445	2514	2566	2642	3037	3073		
	FRA[b]	1531	2682	2697	2994	3122	3390	4165	4451
	Kant.[a]	1455	2520	2639	2662	3187	3146	–	–
	FEM[d]	1449	2511	2567	2637	3037	3061	3917	4225

[a] Kantorovich method [29]
[b] Forced response analysis 1 [28]
[c] Forced response analysis 2 [27]
[d] finite element solution using `NASTRAN`[28]
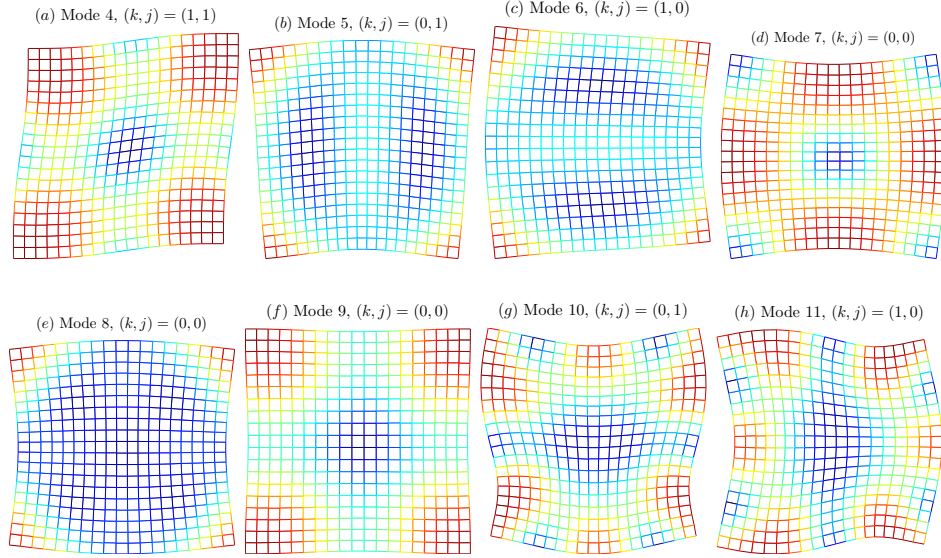[e] Fourier series based analytical method [32]

Figure 4: The first eight non-zero free inplane vibration mode shapes of a completely free square ($a/b = 1$) isotropic plate. The (k, j) notation and the meaning of colour of mesh is the same as those in Table 3.

Next, the current SDSM is used to revisit another interesting problem covered in the literature [27–29, 32]. This is about a plate with three different combinations of free and clamped boundary conditions. The plate is made of material with Young's modulus $E = 7.0 \times 10^{10} \, N/m^2$, Poisson's ratio $\nu = 0.33$ and density $\rho = 2700 \, kg/m^3$, and has dimension $2a \times 2b = 1.0 \, m \times 1.2 \, m$, thickness $h = 2.5 \, mm$. The computed SDSM results are accurate up to the last figures quoted. These results are compared to those computed by Kantorovich method [29], forced response analysis based on two different formulations [27, 28], the Fourier series based analytical method [32] and the finite element solutions by using NASTRAN taken from [28]. It is found that the results obtained by the forced response analysis in [27] and Fourier series based analytical methods [32] match better with the current SDSM compared to the other three methods. The Kantorovich method [29], being a weak formulation, always give upper bound solution of the SDSM results, as expected.

As mentioned earlier, extensive investigations on transverse free vibration of plates have been performed by many authors using different methods. For example, Leissa [1] and more recently Monterrubio and Ilanko [45] gave the free *transverse* vibration results for all 55 possible combination of classical BC for a square isotropic plate. However, there are very few results available for free inplane vibration of plates with limited BCs. To the best of the authors' knowledge, there has not been any meaningful research which provides systematic results for

27

the modal analysis of free inplane vibrating rectangular plates. To fill this gap, a systematic analysis of free inplane vibration of square plates with respected to 55 all possible combination of BCs for free inplane vibration in an efficient manner, see Table 6. These 55 different cases can be categorised into the following two groups.

(i) Cases 1-27 have at least one pair of opposite edges being either S_2-S_2 (Cases 1-10), or S_1-S_1 (Cases 11-19) or S_1-S_2 (Cases 20-27), whose results are shown in the first three sub-parts of Table 6. All SDSM results with S_1-S_1 (Cases 11-19) and S_1-S_2 (Cases 20-27) opposite edges coincide with the closed-form exact solution given by Liu and Xing [20]. It is worth highlighting that rigid body modes with zero natural frequencies exist in cases FS_1FS_1, $S_2S_1FS_1$, $S_2S_1S_2S_1$, $S_2S_1S_2F$ and S_2FS_2F.

(ii) Cases 28-55 have no closed-form exact solution available due to the coupling of translational and shear deformation, whose series-based exact solutions are given in the last section of Table 6 computed by the current method. Note that the FFFF and S_1FFF cases have three and two rigid body modes respectively and Cases S_1S_1FF, S_2S_1FF and S_2FFF have one rigid body mode each.

All SDSM results given in this table have six significant figures (accurate up to the last figure quoted) which will serve as benchmark solutions.

Table 6: Dimensionless natural frequency parameters of free inplane vibration of a square plate (plane stress) with the 55 possible combinations of boundary conditions including free (F), clamped (C) and two simply supported (S_1 and S_2) conditions. All results are presented with six significant figures.

BC	$\lambda = 2\omega a/\pi\sqrt{\rho/G}$									
	1	2	3	4	5	6	7	8	9	10
$S_2S_1S_2S_1$	0	1	1.41421	1.69031	2	2.23607	2.23607	2.39046	2.82843	3
$S_2S_1S_2F$	0	.873927	1.41421	1.69031	1.82440	1.85577	2.17233	2.31659	2.74761	2.77719
S_2FS_2F	0	.757300	1.41421	1.69031	1.74786	1.80990	1.88247	2.00828	2.70899	2.70951
$S_2S_2S_2S_2$	1.41421	1.69031	1.69031	2.23607	2.23607	2.39046	2.82843	3.16228	3.16228	3.38062
$S_2S_2S_2S_1$	.845154	1.11803	1.80278	1.88982	2.06155	2.5	2.53546	2.69258	3.04138	3.04725
$S_2S_2S_2F$	.845154	1.00414	1.64609	1.84184	1.84285	2.29117	2.47970	2.53546	2.74970	2.90811
$S_2CS_2S_1$	.845154	1.18653	1.84116	2.07975	2.28188	2.53546	2.59612	2.93189	3.04928	3.26856
$S_2CS_2S_2$	1.51221	1.69031	1.85646	2.29452	2.32818	2.76014	2.94011	3.19100	3.38062	3.44276
S_2CS_2C	1.69031	1.76220	1.88026	2.37306	2.66720	3.02442	3.02857	3.22709	3.38062	3.68231
S_2CS_2F	.845154	1.06399	1.64723	1.85036	2.23956	2.40021	2.53546	2.58759	2.75074	3.22178
FS_1FS_1	0	.757300	1	1.41421	1.74786	1.80990	1.88247	2	2.00828	2.70899
$S_2S_1FS_1$	0	1	1.00414	1.64609	1.84285	2	2.29117	2.47970	2.74970	
$S_1S_1S_1S_1$	1	1	1.41421	2	2	2.23607	2.23607	2.39046	2.82843	3
$S_2S_1S_1S_1$	0.5	1.11803	1.5	1.80278	1.88982	2.06155	2.5	2.5	2.69258	3.04138
$S_1S_1FS_1$	0.5	.873927	1.41421	1.5	1.82440	1.85577	2.17233	2.31659	2.5	2.74761
$CS_1S_1S_1$	1	1.18653	1.84116	2	2.07975	2.28188	2.59612	2.93189	3	3.04927
$CS_1S_2S_1$	0.5	1.5	1.51221	1.85646	2.29452	2.32818	2.5	2.76014	2.94011	3.19100
CS_1CS_1	1	1.76220	1.88026	2	2.37306	2.66720	3	3.02442	3.02856	3.22709
CS_1FS_1	0.5	1.06399	1.5	1.64723	1.85037	2.23956	2.40021	2.5	2.58759	2.75074
$S_2S_2S_1S_1$	.707107	1.19523	1.58114	1.58114	2.12132	2.54951	2.54951	2.67261	2.67261	2.91548
$S_2S_1S_1F$	.378650	.941233	1.35475	1.49367	1.76722	1.93008	2.28756	2.43779	2.55662	2.61850
$S_2S_2S_1F$	.707107	.904949	1.35449	1.40252	2.04510	2.12132	2.29371	2.53102	2.65621	2.79013
S_2CS_1F	.860033	.946752	1.42583	1.74200	2.21926	2.29673	2.36097	2.75171	2.79317	2.82070
S_2FS_1F	.276567	.796526	1.25564	1.31495	1.60687	1.68775	2.23212	2.25779	2.38948	2.42445
$CS_2S_1S_1$	.881101	1.33360	1.61354	2.04957	2.23446	2.56102	2.66048	2.79136	2.98886	3.05748
$CS_2S_2S_1$	.940128	1.51428	1.89004	1.92102	2.51908	2.55466	2.73266	2.75266	3.18578	3.30205
CS_2CS_1	1.28380	1.66297	2.01761	2.22350	2.51968	2.78449	2.98159	3.18263	3.23935	3.40647
FFFF	0	0	0	1.24858	1.32984	1.32984	1.41421	1.60734	1.85745	2.00319
S_1FFF	0	0	.878906	1.27148	1.41421	1.44333	1.81566	1.84467	2.00440	2.13652
S_1S_1FF	0	.624289	1.15762	1.41421	1.42226	1.84076	1.85649	2.09904	2.22300	2.43273
S_2S_1FF	0	.664917	1.00160	1.33667	1.64088	1.75252	1.87396	2.12165	2.36880	2.42507
S_2FFF	0	.525573	.796522	1.28703	1.40011	1.65355	1.73452	1.77391	2.33104	2.40178
S_2S_2FF	.707107	.803669	.928726	1.35734	1.62575	2.00999	2.12132	2.50031	2.53522	2.54821
CS_1S_1F	.839454	1.00701	1.55971	1.80264	1.90621	2.22052	2.48554	2.57881	2.74932	2.79061
CS_1S_2F	.455469	1.37033	1.50496	1.78844	1.93483	2.25224	2.36007	2.63402	2.80814	2.94807
CS_1CF	0.95428	1.65619	1.82862	1.84274	2.09265	2.52443	2.78711	2.85969	3.00475	3.02279
CS_1FF	.419667	.864225	1.19553	1.57043	1.65165	2.03228	2.19197	2.35016	2.44514	2.56180
CS_2S_1F	.811859	1.04983	1.36949	1.87271	2.06533	2.24415	2.53657	2.68975	2.77951	2.86851
CS_2S_2F	.901419	1.42058	1.66756	1.87598	2.26048	2.38362	2.51471	2.74297	3.03747	3.18318
CS_2CF	1.21704	1.63944	1.73912	2.05996	2.44058	2.50237	2.78395	3.04201	3.18974	3.30536
CS_2FF	.780195	.866792	1.04883	1.53192	1.90485	2.19056	2.22056	2.53739	2.58887	2.73934
CCS_1S_1	1.13931	1.39506	2.04362	2.09845	2.34596	2.79871	2.81142	3.05389	3.06575	3.21783
CCS_1F	.952706	1.12156	1.71331	1.90894	2.26837	2.48920	2.71018	2.77972	2.86280	2.89448
CCS_2S_1	.956421	1.58572	1.91359	2.30920	2.54354	2.58552	2.79394	3.09703	3.30431	3.36484
CCS_2S_2	1.57609	1.80451	1.95877	2.34534	2.69570	2.84250	3.04628	3.43399	3.45755	3.56133
CCS_2F	.918699	1.46666	1.67429	2.19408	2.36998	2.44756	2.56184	2.90484	3.17449	3.29829
$CCCS_1$	1.28835	1.80570	2.18988	2.42064	2.55989	3.01154	3.11275	3.27972	3.32108	3.46010
$CCCS_2$	1.71597	1.89626	2.04679	2.61396	2.85183	3.02734	3.15932	3.47830	3.61595	3.72833
CCCC	1.91284	1.91284	2.27861	2.79012	3.15219	3.17144	3.17144	3.60901	3.82718	3.82718
CCCF	1.22128	1.70181	1.83415	2.31670	2.53854	2.66737	2.80092	3.20792	3.24602	3.44820
CCFF	.790796	1.01362	1.21300	1.83061	2.06761	2.27608	2.32899	2.66579	2.76446	2.83639
CFS_1F	.799249	.810760	1.31601	1.64507	1.77689	2.01372	2.28471	2.47004	2.53222	2.73372
CFS_2F	.406378	1.27806	1.49670	1.75314	1.87776	1.89279	2.26359	2.39156	2.73271	2.88667
CFCF	.910936	1.62372	1.67891	1.80284	2.01402	2.09965	2.73897	2.74065	2.84116	3.00993
CFFF	.337798	.810700	.909521	1.44529	1.55856	1.65413	2.08498	2.19502	2.42378	2.43925

3.3. Applications to plane strain problems

Plane strain vibration is also very important in engineering applications such as structural health monitoring and earthquake engineering as mentioned earlier in the Introduction section.

Similar to but different from Table 6, Table 7 tabulates the SDS results of all 55 possible combinations of BCs for an isotropic solid under free plane strain vibra-

29

Table 7: The same as for Fig. 6 except that the results in this table are for an isotropic solid subject to 55 possible BCs and under free plane strain vibration. All results are presented with six significant figures.

BC	$\lambda = 2\omega a/\pi\sqrt{\rho/G}$									
	1	2	3	4	5	6	7	8	9	10
$S_2S_1S_2S_1$	0	1	1.41421	1.87083	2	2.23607	2.23607	2.64575	2.82843	3
$S_2S_1S_2F$	0	.886170	1.41421	1.84589	1.87083	1.93400	2.17646	2.46570	2.78086	2.82843
S_2FS_2F	0	.774502	1.41421	1.77234	1.87083	1.90726	2.00123	2.03558	2.74193	2.82554
$S_2S_2S_2S_2$	1.41421	1.87083	1.87083	2.23607	2.23607	2.64575	2.82843	3.16228	3.16228	3.60555
$S_2S_2S_2S_1$	.935414	1.11803	1.80278	2.06155	2.09165	2.5	2.69258	2.80624	3.04138	3.20156
$S_2S_2S_2F$	.935414	1.01779	1.70182	1.86568	1.98262	2.35949	2.48178	2.78366	2.80624	3.05740
$S_2CS_2S_1$	.935414	1.19256	1.91350	2.08091	2.36975	2.60683	2.80624	3.04973	3.05974	3.33901
$S_2CS_2S_2$	1.54536	1.87083	1.98540	2.29906	2.45687	2.85664	2.96377	3.19278	3.61254	3.67074
S_2CS_2C	1.80552	1.87083	2.00089	2.38512	2.82559	3.07972	3.09071	3.23171	3.74166	3.79862
S_2CS_2F	.935414	1.09159	1.71790	1.87586	2.33436	2.50563	2.59934	2.78501	2.80624	3.30287
FS_1FS_1	0	.774502	1	1.41421	1.77234	1.90726	2	2	2.03558	2.74193
$S_2S_1FS_1$	0	1	1.01779	1.70182	1.86568	1.98262	2	2.35949	2.48179	2.78366
$S_1S_1S_1S_1$	1	1	1.41421	2	2	2.23607	2.23607	2.64575	2.82843	3
$S_2S_1S_1S_1$	0.5	1.11803	1.5	1.80278	2.06155	2.09165	2.5	2.5	2.69258	3.04138
$S_1S_1FS_1$	0.5	.886170	1.41421	1.5	1.84589	1.93400	2.17646	2.46569	2.5	2.78087
$CS_1S_1S_1$	1	1.19256	1.91350	2	2.08091	2.36975	2.60683	3	3	3.05974
$CS_1S_2S_1$	0.5	1.5	1.54536	1.98540	2.29906	2.45687	2.5	2.85664	2.96377	3.19278
CS_1CS_1	1	1.80552	2	2	2.38512	2.82559	3	3.07972	3.09071	3.23171
CS_1FS_1	0.5	1.09159	1.5	1.71790	1.87586	2.33436	2.5	2.5	2.59934	2.78501
$S_2S_2S_1S_1$	.707107	1.32288	1.58114	1.58114	2.12132	2.54951	2.54951	2.91548	2.91548	2.95804
$S_2S_1S_1F$	.387251	.953628	1.37096	1.53859	1.77049	2.08592	2.31491	2.45497	2.57172	2.62198
$S_2S_2S_1F$	.707107	1.000613	1.41277	1.42165	2.06381	2.12132	2.32247	2.69636	2.87526	2.88716
S_2CS_1F	.902469	1.002895	1.44932	1.78486	2.24616	2.32619	2.43692	2.85407	2.96252	2.99036
S_2FS_1F	.286010	.825215	1.27690	1.32947	1.70532	1.73912	2.26021	2.33302	2.42276	2.43447
$CS_2S_1S_1$	.902762	1.41280	1.61586	2.06362	2.25860	2.56170	2.89247	2.93410	2.99502	3.10269
$CS_2S_2S_1$	1.000445	1.53986	1.89931	2.08635	2.56960	2.61618	2.73536	2.94661	3.31388	3.36403
CS_2CS_1	1.33327	1.75109	2.03972	2.32213	2.65368	2.79166	3.00376	3.36145	3.36403	3.43770
FFFF	0	0	0	1.25290	1.37893	1.37893	1.41421	1.67942	2.02200	2.02200
S_1FFF	0	0	.892215	1.28832	1.41421	1.49753	1.87372	2.00105	2.02398	2.17155
S_1S_1FF	0	.626450	1.18516	1.41421	1.44463	1.88488	1.92596	2.13364	2.37303	2.44641
S_2S_1FF	0	.689463	1.01100	1.36630	1.68545	1.82978	1.97443	2.16120	2.40967	2.44953
S_2FFF	0	.546239	.825200	1.30582	1.45686	1.71237	1.75972	1.91124	2.37796	2.41768
S_2S_2FF	.707107	.839709	1.046181	1.39887	1.66037	2.03908	2.12132	2.56908	2.66536	2.66826
CS_1S_1F	.861695	1.02134	1.58338	1.83648	1.94719	2.29804	2.52066	2.59751	2.80470	2.93115
CS_1S_2F	.458948	1.38712	1.53545	1.92812	2.00084	2.31524	2.42468	2.66622	2.88054	2.97290
CS_1CF	.958235	1.73226	1.84845	1.96669	2.31893	2.62982	2.82344	2.92097	3.04468	3.08345
CS_1FF	.426539	.898669	1.22124	1.58778	1.71947	2.08232	2.27530	2.41474	2.51748	2.58120
CS_2S_1F	.851653	1.09459	1.42220	1.90089	2.08145	2.26252	2.73058	2.76128	2.88940	2.99395
CS_2S_2F	.965629	1.44595	1.75527	1.99133	2.30005	2.43830	2.61430	2.91931	3.11868	3.23496
CS_2CF	1.27369	1.71773	1.81807	2.14614	2.48352	2.63162	2.82748	3.14301	3.31249	3.38665
CS_2FF	.806586	.936924	1.09784	1.57387	1.94083	2.23164	2.25118	2.65363	2.72780	2.87327
CCS_1S_1	1.14151	1.46857	2.04724	2.11462	2.39225	2.91611	2.96485	3.07097	3.09394	3.34217
CCS_1F	.996842	1.16059	1.74394	1.94545	2.32378	2.52383	2.76441	2.91311	3.01443	3.01755
CCS_2S_1	1.02172	1.59626	1.99532	2.37229	2.58332	2.70319	2.94840	3.14349	3.43664	3.44308
CCS_2S_2	1.64900	1.96896	2.03949	2.44636	2.70960	2.93694	3.09538	3.59505	3.66399	3.72085
CCS_2F	.989362	1.49175	1.76270	2.25570	2.43506	2.53755	2.71528	2.99337	3.24043	3.38483
$CCCS_1$	1.33887	1.85710	2.23298	2.48627	2.71080	3.02782	3.17454	3.38102	3.44897	3.57579
$CCCS_2$	1.84360	2.02164	2.09991	2.68364	2.94423	3.08440	3.24572	3.65886	3.76425	3.91724
CCCC	2.04343	2.04343	2.28302	2.93715	3.19252	3.19252	3.29800	3.93791	3.99063	3.99063
CCCF	1.27899	1.79281	1.86972	2.41536	2.67461	2.70193	2.85773	3.31911	3.39448	3.54525
CCFF	.824049	1.09393	1.23250	1.87535	2.10789	2.33315	2.37578	2.84730	2.89610	2.99418
CFS_1F	.811771	.853527	1.33557	1.72341	1.79899	2.03481	2.35903	2.50107	2.72982	2.76279
CFS_2F	.413047	1.29777	1.52462	1.91964	1.93112	2.01384	2.28787	2.43271	2.83645	2.91838
CFCF	.917896	1.70331	1.72339	1.93126	2.04268	2.18917	2.77425	2.84441	2.89191	3.07090
CFFF	.347924	.853425	.933513	1.49982	1.56978	1.73434	2.13267	2.29389	2.46131	2.47801

tion whose cross section is a square. All results are presented with six significant figures which will serve as benchmark solutions. A comparison between Tables 6 and 7 will lead to the conclusion that the natural frequencies under plane strain vibrations are always slightly higher than those under plane stress vibrations as expected. This agrees with the qualitative prediction made earlier after Eq. (5) in Section 2.1. As it appears, there is no literature which mentions the closed-form exact solution for plane strain vibration problems. Nevertheless, it is not difficult to realise that closed-form exact solutions for Cases 1-27 undergoing plane

strain vibration can easily be obtained by slightly modifying the closed-form exact solutions [20] for the corresponding plane stress cases.

The current SDSM allows the modelling of the plane strain vibration problems of solids with complex cross section just by assembling the corresponding SDS elements directly. In this paper, three engineering cases of practical significance are investigated as illustrative examples, see Fig. 5. Case 1 (Fig. 5(a)) is an infinite aluminium thick plate ($E = 70\,GPa$, $\nu = 0.3$, and $\rho = 2700\,kg/m^3$) with a step in the thickness. The plate is cantilevered on the left edge and free on all other surfaces and edges. Case 2 (Fig. 5(b)) is an infinite plate clamped at the two opposite edges while stiffened by an infinite steel ($E = 210\,GPa$, $\nu = 0.3$, $\rho = 7800\,kg/m^3$) beam in the middle with square cross section. Case 3 (Fig. 5(c)) is an infinite concrete shear wall ($E = 17\,GPa$, $\nu = 0.2$, $\rho = 7800\,kg/m^3$) fixed on its feet. All three cases are assumed to vibrate freely under plane strain deformation in which the deformation is assumed to be uniform in the infinite direction. The first two problems (Fig. 5(a) and (b)) are ideal models to study the interaction between plane vibration (in the form of plane waves, e.g., shear horizontal waves and Lamb waves) and defects and discontinuities (e.g., thickness step or junctions) whereas the third problem is a suitable model to investigate dynamic behaviour of shear wall subject to seismic or wind loads. The first ten natural frequencies computed by the current SDSM are included in Table 8, which are also compared with those obtained by the FEM software ANSYS. Three, four and five SDS elements are used respectively for Cases 1, 2 and 3 whereas about 10^5 Plane 182 elements were adopted in the FEM modelling. All SDSM results are accurate up to the last figures which all agree well with the FE solutions. The first six mode shapes of Cases 2 and 3 are shown in Figs. 6 and 7.
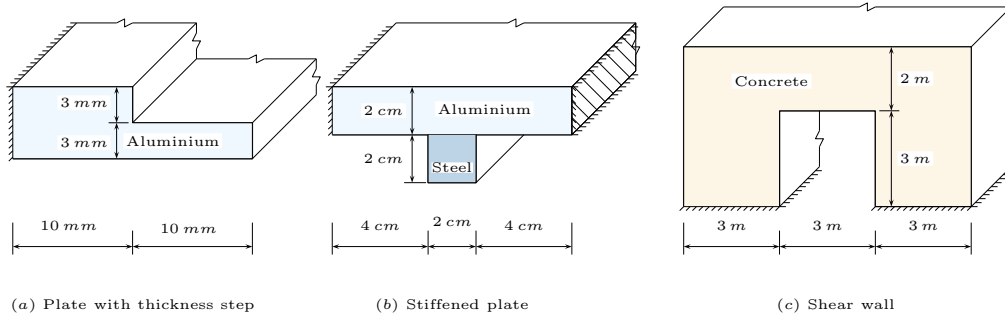

(a) Plate with thickness step (b) Stiffened plate (c) Shear wall

Figure 5: Three cases under plane strain vibration. (a) is a cantilever infinite aluminium plate with thickness step, (b) is an infinite aluminium plate clamped along two opposite edges and stiffened by an infinite steel beam with square cross section, and (c) depicts an infinite concrete shear wall clamped on its feet.

31

Table 8: The first ten natural frequencies of three cases described in Fig. 5 undergoing plane strain vibration. The results are computed by using two methods, the current SDSM and the finite element software `ANSYS`.

Cases	Methods	1	2	3	4	5	6	7	8	9	10
Case 1 (kHz)	SDSM	**13.37**	**42.77**	**76.78**	**104.2**	**154.7**	**184.2**	**236.9**	**289.4**	**327.7**	**339.2**
	FEM	13.38	42.79	76.78	104.2	154.8	184.2	237.1	289.5	327.7	339.2
Case 2 (kHz)	SDSM	**6.132**	**9.269**	**22.82**	**28.43**	**30.68**	**49.17**	**50.69**	**53.83**	**58.64**	**72.60**
	FEM	6.135	9.281	22.82	28.46	30.70	49.17	50.69	53.85	58.67	72.60
Case 3 (Hz)	SDSM	**47.37**	**99.01**	**132.9**	**136.4**	**147.4**	**176.9**	**234.9**	**274.2**	**306.6**	**326.8**
	FEM	47.39	99.05	132.9	136.4	147.4	176.9	235.0	274.3	306.6	326.9
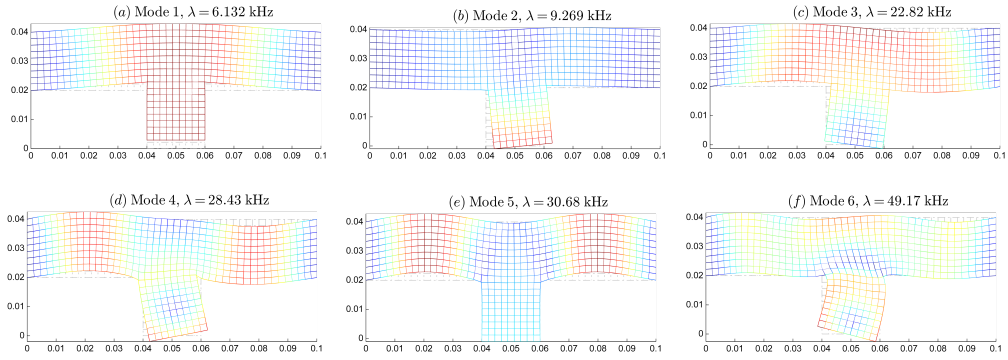
Figure 6: The first six natural plane strain mode shapes of an aluminium plate stiffened by a steel beam with square cross-section. The colour of the mesh is the same as Fig. 3.
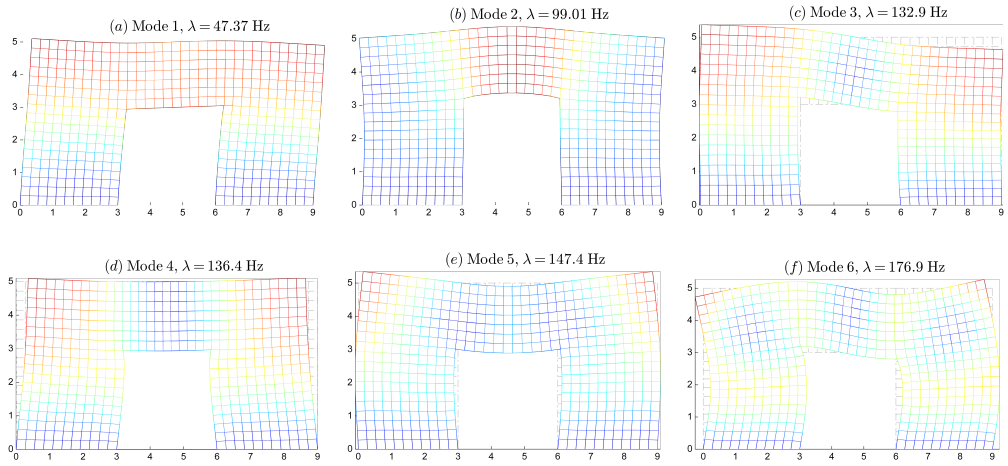
Figure 7: The first six natural mode shapes of a concrete shear wall under plane strain vibration.

Due to the vertical symmetrical geometries of Cases 2 and 3, the mode shapes of both cases are obviously either symmetric or antisymmetric. In Fig. 6, modes

32

1 and 5 are symmetric whereas the other four modes are antisymmetric. In Fig. 7, modes 2, 4 and 5 are symmetric and the remaining modes are antisymmetric. Of course, the current SDSM can be applied to more complex geometries by assembling the corresponding SDS matrices.

4. Conclusions

The spectral dynamic stiffness (SDS) formation for plane elastodynamic problems has been developed which covers both plane stress and plane strain vibrations. The method essentially provides a highly efficient and accurate modelling tool for plane elastodynamic problems by a very small number of DOF. The formulation is in a strong form which is based on the exact general solution derived from the governing differential equation by using two types of modified Fourier series. The developed spectral dynamic stiffness elements can be assembled directly to model simple as well as complex geometries. Any arbitrary boundary conditions can be accounted for in the form of modified Fourier series. As a solution technique, the Wittrick-Williams algorithm is applied with considerable enhancement to overcome the troublesome J_0 count problem in an elegant way. As a result, plane elastodynamic problems with complex geometries can be modelled by as few SDS elements as possible. Any required natural frequencies covering low, medium to high frequency ranges can be computed up to any desired accuracy by the proposed method. Benchmark solutions have been presented in this paper both for classical cases as well as for a wide range of engineering problems undergoing both plane stress and plane strain vibrations. The computational efficiency and analytical elegance of the proposed method make it an ideal tool for parametric studies and optimization analyses.

Note that the SDS formulation developed can also be used for dynamic response and wave propagation problems, which will facilitate many important engineering applications such as structural health monitoring, acoustic transmission modelling and many others. Besides, although the proposed method already has the excellent computational efficiency, it could be sped-up even further by incorporating the substructuring techniques, e.g., [46]. Furthermore, the framework of the SDS method generalised in this paper has paved the way for the SDS formulation for other types of Helmholtz equations or Maxwell equations.

Appendix A. Two sets of modified Fourier basis functions and the modified Fourier expansion of hyperbolic functions

Two types of modified Fourier basis functions (MFBF) given in Eqs. (16) and (17) are illustrated in Table A.1, where the first three functions are shown.

Table A.1: The first three Fourier basis functions $\mathcal{T}_l(\gamma_{ls}\xi)$ and their conjugates $\mathcal{T}_l^*(\gamma_{ls}\xi)$.

$\mathcal{T}_l(\gamma_{ls}\xi)$	$s = 0$	$s = 1$	$s = 2$
$\mathcal{T}_0(\gamma_{0s}\xi)$			
$\mathcal{T}_1(\gamma_{1s}\xi)$			
$\mathcal{T}_0^*(\gamma_{0s}\xi)$			
$\mathcal{T}_1^*(\gamma_{1s}\xi)$			

Following the MFS given in Eqs. (18) and (20), the hyperbolic functions $\mathcal{H}_l(\Gamma\xi)$ and its conjugate $\mathcal{H}_l^*(\Gamma\xi)$ in Eq. (30) can be transformed into MFS by using Eqs. (18) and (20), respectively. In this way,

$$\mathcal{H}_l(\Gamma\xi) = \sum_{s\in\mathbb{N}} \frac{2(-1)^s \Gamma \mathcal{H}_l^*(\Gamma L)}{\sqrt{\zeta_{ls}L}(\Gamma^2 + \gamma_{ls}^2)} \frac{\mathcal{T}_l(\gamma_{ls}\xi)}{\sqrt{\zeta_{ls}L}} , \tag{A.1a}$$

$$\mathcal{H}_l^*(\Gamma\xi) = \sum_{s\in\mathbb{N}} \frac{2(-1)^{s+l+1} \gamma_{ls} \mathcal{H}_l^*(\Gamma L)}{\sqrt{\zeta_{ls}L}(\Gamma^2 + \gamma_{ls}^2)} \frac{\mathcal{T}_l^*(\gamma_{ls}\xi)}{\sqrt{\zeta_{ls}L}} , \tag{A.1b}$$

where the function $\mathcal{H}_l^*(\cdot)$ was defined in Eq. (30b).

Appendix B. The relationship between arbitrary boundary conditions and their kj components

Considering the symmetry/antisymmetry of U^{kj} and V^{kj} of Eq. (29) and their derivatives, the relationships between the boundary conditions (BCs) in Eq. (15) and their four kj components in Eq. (C.1) are as follows

$$
\begin{bmatrix} L_1 \\ \phi_1 \\ L_2 \\ \phi_2 \\ L_3 \\ \phi_3 \\ L_4 \\ \phi_4 \end{bmatrix} = \begin{bmatrix} L_a^{00} + L_a^{01} + L_a^{10} + L_a^{11} \\ T_a^{00} + T_a^{01} + T_a^{10} + T_a^{11} \\ L_b^{00} + L_b^{01} + L_b^{10} + L_b^{11} \\ T_b^{00} + T_b^{01} + T_b^{10} + T_b^{11} \\ -L_a^{00} - L_a^{01} + L_a^{10} + L_a^{11} \\ T_a^{00} + T_a^{01} - T_a^{10} - T_a^{11} \\ -L_b^{00} + L_b^{01} - L_b^{10} + L_b^{11} \\ T_b^{00} - T_b^{01} + T_b^{10} - T_b^{11} \end{bmatrix}, \quad \begin{bmatrix} N_1 \\ S_1 \\ N_2 \\ S_2 \\ N_3 \\ S_3 \\ N_4 \\ S_4 \end{bmatrix} = \begin{bmatrix} N_a^{00} + N_a^{01} + N_a^{10} + N_a^{11} \\ S_a^{00} + S_a^{01} + S_a^{10} + S_a^{11} \\ N_b^{00} + N_b^{01} + N_b^{10} + N_b^{11} \\ S_b^{00} + S_b^{01} + S_b^{10} + S_b^{11} \\ -N_a^{00} - N_a^{01} + N_a^{10} + N_a^{11} \\ S_a^{00} + S_a^{01} - S_a^{10} - S_a^{11} \\ -N_b^{00} + N_b^{01} - N_b^{10} + N_b^{11} \\ S_b^{00} - S_b^{01} + S_b^{10} - S_b^{11} \end{bmatrix}. \quad \text{(B.1)}
$$

It should be noted that any prescribed BC on the left-hand sides of Eq. (B.1) can be decomposed into a symmetric and an antisymmetric components, e.g., $L_i = L_i^0 + L_i^1$ and $N_i = N_i^0 + N_i^1$ with subscript '0' or '1' denoting the symmetric or the antisymmetric component respectively. Equating the symmetric/antisymmetric components of both sides of Eq. (B.1) leads to

$$[L_1^0, L_1^1, L_3^0, L_3^1]^T = \boldsymbol{T}_1 [L_a^{00}, L_a^{01}, L_a^{10}, L_a^{11}]^T \tag{B.2a}$$

$$[L_2^0, L_2^1, L_4^0, L_4^1]^T = \boldsymbol{T}_2 [L_b^{00}, L_b^{01}, L_b^{10}, L_b^{11}]^T \tag{B.2b}$$

$$[T_1^0, T_1^1, T_3^0, T_3^1]^T = \boldsymbol{T}_3 [T_a^{00}, T_a^{01}, T_a^{10}, T_a^{11}]^T \tag{B.2c}$$

$$[T_2^0, T_2^1, T_4^0, T_4^1]^T = \boldsymbol{T}_4 [T_b^{00}, T_b^{01}, T_b^{10}, T_b^{11}]^T \tag{B.2d}$$

and

$$[N_1^0, N_1^1, N_3^0, N_3^1]^T = \boldsymbol{T}_1 [N_a^{00}, N_a^{01}, N_a^{10}, N_a^{11}]^T \tag{B.3a}$$

$$[N_2^0, N_2^1, N_4^0, N_4^1]^T = \boldsymbol{T}_2 [N_b^{00}, N_b^{01}, N_b^{10}, N_b^{11}]^T \tag{B.3b}$$

$$[S_1^0, S_1^1, S_3^0, S_3^1]^T = \boldsymbol{T}_3 [S_a^{00}, S_a^{01}, S_a^{10}, S_a^{11}]^T \tag{B.3c}$$

$$[S_2^0, S_2^1, S_4^0, S_4^1]^T = \boldsymbol{T}_4 [S_b^{00}, S_b^{01}, S_b^{10}, S_b^{11}]^T. \tag{B.3d}$$

In Eqs. (B.2) and (B.3),

$$
\boldsymbol{T}_1 = \begin{bmatrix} 1 & 0 & 1 & 0 \\ 0 & 1 & 0 & 1 \\ -1 & 0 & 1 & 0 \\ 0 & -1 & 0 & 1 \end{bmatrix}, \quad \boldsymbol{T}_2 = \begin{bmatrix} 1 & 1 & 0 & 0 \\ 0 & 0 & 1 & 1 \\ -1 & 1 & 0 & 0 \\ 0 & 0 & -1 & 1 \end{bmatrix}, \tag{B.4a}
$$

$$
\boldsymbol{T}_3 = \begin{bmatrix} 1 & 0 & 1 & 0 \\ 0 & 1 & 0 & 1 \\ 1 & 0 & -1 & 0 \\ 0 & 1 & 0 & -1 \end{bmatrix}, \quad \boldsymbol{T}_4 = \begin{bmatrix} 1 & 1 & 0 & 0 \\ 0 & 0 & 1 & 1 \\ 1 & -1 & 0 & 0 \\ 0 & 0 & 1 & -1 \end{bmatrix}, \tag{B.4b}
$$

where $\boldsymbol{T}_\tau^{-1} = \boldsymbol{T}_\tau^T / 2 \,(\tau = 1, 2, 3, 4)$.

Appendix C. Determination of the unknowns in the general solutions

The entries in Eq. (35) can be expressed either by substituting Eq. (29) into the corresponding BCs or by expressing them using the two types of modified Fourier series (MFS) given in Eqs. (18) and (20), namely

$$
\begin{bmatrix} L_a^{kj} \\[2mm] L_b^{kj} \\[2mm] T_a^{kj} \\[2mm] T_b^{kj} \end{bmatrix} = \begin{bmatrix} U^{kj}|_{x=a} \\[2mm] V^{kj}|_{y=b} \\[2mm] V^{kj}|_{x=a} \\[2mm] U^{kj}|_{y=b} \end{bmatrix} = \begin{bmatrix} \displaystyle\sum_{n\in\mathbb{N}} L_{ajn}\frac{\mathcal{T}_j(\beta_{jn}y)}{\sqrt{\zeta_{jn}b}} \\[3mm] \displaystyle\sum_{m\in\mathbb{N}} L_{bkm}\frac{\mathcal{T}_k(\alpha_{km}x)}{\sqrt{\zeta_{km}a}} \\[3mm] \displaystyle\sum_{n\in\mathbb{N}} T_{ajn}\frac{\mathcal{T}_j^*(\beta_{jn}y)}{\sqrt{\zeta_{jn}b}} \\[3mm] \displaystyle\sum_{m\in\mathbb{N}} T_{bkm}\frac{\mathcal{T}_k^*(\alpha_{km}x)}{\sqrt{\zeta_{km}a}} \end{bmatrix}, \tag{C.1a}
$$

$$
\begin{bmatrix} N_a^{kj} \\[2mm] N_b^{kj} \\[2mm] S_a^{kj} \\[2mm] S_b^{kj} \end{bmatrix} = G \begin{bmatrix} a_1(U_{,x}^{kj} + \nu V_{,y}^{kj})|_{x=a} \\[2mm] a_1(V_{,y}^{kj} + \nu U_{,x}^{kj})|_{y=b} \\[2mm] U_{,y}^{kj} + V_{,x}^{kj}|_{x=a} \\[2mm] U_{,y}^{kj} + V_{,x}^{kj}|_{y=b} \end{bmatrix} = G \begin{bmatrix} \displaystyle\sum_{n\in\mathbb{N}} N_{ajn}\frac{\mathcal{T}_j(\beta_{jn}y)}{\sqrt{\zeta_{jn}b}} \\[3mm] \displaystyle\sum_{m\in\mathbb{N}} N_{bkm}\frac{\mathcal{T}_k(\alpha_{km}x)}{\sqrt{\zeta_{km}a}} \\[3mm] \displaystyle\sum_{n\in\mathbb{N}} S_{ajn}\frac{\mathcal{T}_j^*(\beta_{jn}y)}{\sqrt{\zeta_{jn}b}} \\[3mm] \displaystyle\sum_{m\in\mathbb{N}} S_{bkm}\frac{\mathcal{T}_k^*(\alpha_{km}x)}{\sqrt{\zeta_{km}a}} \end{bmatrix}. \tag{C.1b}
$$

The modified Fourier coefficients $L_{ajn}, L_{bkm}, N_{ajn}, N_{bkm}$ and $T_{ajn}, T_{bkm}, S_{ajn}, S_{bkm}$ are obtained by applying the MFS of Eqs. (18) and (20) respectively. For example,

$$
L_{ajn} = \int_{-b}^{b} L_a^{kj}\frac{\mathcal{T}_j(\beta_{jn}y)}{\sqrt{\zeta_{jn}b}}\mathrm{d}y\,, \quad S_{bkm} = \int_{-a}^{a} \frac{S_b^{kj}}{G}\frac{\mathcal{T}_k^*(\alpha_{km}y)}{\sqrt{\zeta_{km}a}}\mathrm{d}x\,. \tag{C.2}
$$

Next step is to solve the unknowns $C_{00}, C_{1km}, C_{2km}, D_{00}, D_{1jn}$ and D_{2jn} in the general solution of Eq. (29) by using the expressions for L_a^{kj} in Eq. (C.1a) and S_a^{kj} in Eq. (C.1b). Thus, the following equations can be obtained

$$
U^{kj}\big|_{x=a} = \sum_{n\in\mathbb{N}} L_{ajn}\mathcal{T}_j(\beta_{jn}y)/\sqrt{\zeta_{jn}b}\,, \tag{C.3a}
$$

$$
U_{,y}^{kj} + V_{,x}^{kj}\big|_{x=a} = \sum_{n\in\mathbb{N}} S_{ajn}\mathcal{T}_j^*(\beta_{jn}y)/\sqrt{\zeta_{jn}b}\,, \tag{C.3b}
$$

which yield

$$
\sum_{i=1,2} [D_{ijn}\mathcal{H}_k^*(r_{ijn}a)] = L_{ajn}/\sqrt{\zeta_{jn}b}\,, \tag{C.4a}
$$

$$
\sum_{i=1,2} \left[\left((-1)^{j+1}\beta_{jn} + \delta_{ijn}r_{ijn}\right)D_{ijn}\mathcal{H}_k^*(r_{ijn}a)\right] = S_{ajn}/\sqrt{\zeta_{jn}b} \tag{C.4b}
$$

36

$(\forall)$ $k, j \in \{0, 1\}, n \in \mathbb{N}$ except for $n = j = 0$ when Eq. (C.4a) becomes $D_{00}\mathcal{H}_k^*(r_{00}a) = L_{a00}/\sqrt{2b}$. The unknown coefficients D_{00}, D_{1jn} and D_{2jn} can then be determined from Eq. (C.4) to give

$$D_{00} = \frac{L_{a00}}{\sqrt{2b}\mathcal{H}_k^*(r_{00}a)} \qquad\qquad j = n = 0 \qquad \text{(C.5a)}$$

$$\left.\begin{array}{l} D_{1jn} = \dfrac{\left[(-1)^{j+1}\beta_{jn}+\delta_{2jn}r_{2jn}\right]L_{ajn}-S_{ajn}}{\sqrt{\zeta_{jn}}b\mathcal{H}_k^*(r_{1jn}a)\Sigma_2/\mu_2} \\[2ex] D_{2jn} = -\dfrac{\left[(-1)^{j+1}\beta_{jn}+\delta_{1jn}r_{1jn}\right]L_{ajn}-S_{ajn}}{\sqrt{\zeta_{jn}}b\mathcal{H}_k^*(r_{2jn}a)\Sigma_2/\mu_2} \end{array}\right\} \qquad \text{otherwise}, \qquad \text{(C.5b)}$$

where $\Sigma_2 = a_1(r_{1jn}^2 - r_{2jn}^2)$. Similarly, the expressions of L_b^{kj} and S_b^{kj} in Eqs. (C.1a) and (C.1b) yield the unknowns C_{00}, C_{1km} and C_{2km} as

$$C_{00} = \frac{L_{b00}}{\sqrt{2a}\mathcal{H}_j^*(t_{00}b)} \qquad\qquad k = m = 0 \qquad \text{(C.6a)}$$

$$\left.\begin{array}{l} C_{1km} = \dfrac{\left[(-1)^{k+1}\alpha_{km}+\delta_{2km}t_{2km}\right]L_{bkm}-S_{bkm}}{\sqrt{\zeta_{km}}a\mathcal{H}_j^*(t_{1km}b)\Sigma_1/\mu_1} \\[2ex] C_{2km} = -\dfrac{\left[(-1)^{k+1}\alpha_{km}+\delta_{1km}t_{1km}\right]L_{bkm}-S_{bkm}}{\sqrt{\zeta_{km}}a\mathcal{H}_j^*(t_{2km}b)\Sigma_1/\mu_1} \end{array}\right\} \qquad \text{otherwise}, \qquad \text{(C.6b)}$$

where $\Sigma_1 = a_1(t_{1km}^2 - t_{2km}^2)$.

Appendix D. Infinite system of algebraic equations derived from $T_a^{kj}, T_b^{kj}, N_a^{kj}$ and N_b^{kj} of Eqs. (C.1)

By equating the expressions of T_a^{kj}, T_b^{kj} in Eq. (C.1a), the following two relationships are obtained

$$T_a^{kj} = V^{kj}|_{x=a} = \sum_{m\in\mathbb{N}} \left[(-1)^m \sum_{i=1,2} \left(C_{ikm}\mathcal{H}_j^*(t_{ikm}y) \right) \right]$$

$$+ \sum_{n\in\mathbb{N}} \left[\sum_{i=1,2} (\delta_{ijn}D_{ijn}\mathcal{H}_k(r_{ijn}a)) \mathcal{T}_j^*(\beta_{jn}y) \right] = \sum_{n\in\mathbb{N}} T_{ajn}\mathcal{T}_j^*(\beta_{jn}y)/\sqrt{\zeta_{jn}b} \quad \text{(D.1a)}$$

$$T_b^{kj} = U^{kj}|_{y=b} = \sum_{m\in\mathbb{N}} \left[\sum_{i=1,2} (\delta_{ikm}C_{ikm}\mathcal{H}_j(t_{ikm}b)) \mathcal{T}_k^*(\alpha_{km}x) \right]$$

$$+ \sum_{n\in\mathbb{N}} \left[(-1)^n \sum_{i=1,2} (D_{ijn}\mathcal{H}_k^*(r_{ijn}x)) \right] = \sum_{m\in\mathbb{N}} T_{bkm}\mathcal{T}_k^*(\alpha_{km}x)/\sqrt{\zeta_{km}a}. \quad \text{(D.1b)}$$

Now substituting Eqs. (C.5) and (C.6) into Eq. (D.1), applying the MFS (A.1b) to $\mathcal{H}_j^*(t_{ikm}y)$ and $\mathcal{H}_k^*(r_{ijn}x)$ and eliminating the common terms $\mathcal{T}_j^*(\beta_{jn}y)/\sqrt{\zeta_{jn}b}$ or $\mathcal{T}_k^*(\alpha_{km}x)/\sqrt{\zeta_{km}a}$ from both sides, the following infinite system of algebraic equations will be arrived at

$$\sum_{m\in\mathbb{N}} \frac{2(-1)^{m+n+j}\beta_{jn}}{\sqrt{\zeta_{km}\zeta_{jn}}ab\Sigma_1(t_{1km}^2 + \beta_{jn}^2)(t_{2km}^2 + \beta_{jn}^2)} \Big\{ \left[\Gamma_{11}t_{1km}^2 - \Gamma_{12}t_{2km}^2 + (\Gamma_{11} - \Gamma_{12})\beta_{jn}^2\right]L_{bkm}$$

$$- (t_{1km}^2 - t_{2km}^2)S_{bkm} \Big\} + \frac{\mu_2}{\Sigma_2} \Big\{ \left[(\delta_{1jn}\Gamma_{22}\mathcal{P}_k(r_{1jn}a) - \delta_{2jn}\Gamma_{21}\mathcal{P}_k(r_{2jn}a)) L_{ajn} \right.$$

$$\left. - (\delta_{1jn}\mathcal{P}_k(r_{1jn}a) - \delta_{2jn}\mathcal{P}_k(r_{2jn}a)) S_{ajn} \right] \Big\} = T_{ajn} \quad \text{(D.2)}$$

$$\sum_{n\in\mathbb{N}} \frac{2(-1)^{m+n+k}\alpha_{km}}{\sqrt{\zeta_{km}\zeta_{jn}}ab\Sigma_2(r_{1jn}^2 + \alpha_{km}^2)(r_{2jn}^2 + \alpha_{km}^2)} \Big\{ \left[\Gamma_{21}r_{1jn}^2 - \Gamma_{22}r_{2jn}^2 + (\Gamma_{21} - \Gamma_{22})\alpha_{km}^2\right]L_{ajn}$$

$$- (r_{1jn}^2 - r_{2jn}^2)S_{ajn} \Big\} + \frac{\mu_1}{\Sigma_1} \Big\{ \left[\delta_{1km}\Gamma_{12}\mathcal{P}_j(t_{1km}b) - \delta_{2km}\Gamma_{11}\mathcal{P}_j(t_{2km}b)\right]L_{bkm}$$

$$- \left[\delta_{1km}\mathcal{P}_j(t_{1km}b) - \delta_{2km}\mathcal{P}_j(t_{2km}b)\right]S_{bkm} \Big\} = T_{bkm}. \quad \text{(D.3)}$$

in which $\mathcal{P}_l(\Xi) = \mathcal{H}_l(\Xi)/\mathcal{H}_l^*(\Xi)$. Similar procedure can be carried out for N_a^{kj} N_b^{kj} in Eq. (C.1b) which will lead to another set of infinite algebraic system.

Appendix E. Expressions of the coefficient matrices in the mixed-variable formulation of Eq. (36)

The analytical expressions for the coefficient matrices in Eq. (36) are given in this appendix. After symbolic manipulation, the four coefficient matrices $\boldsymbol{A}_{TL}^{kj}$, $\boldsymbol{A}_{TS}^{kj}$, $\boldsymbol{A}_{NL}^{kj}$ and $\boldsymbol{A}_{NS}^{kj}$ can be expressed in an extremely concise form. The following expressions are the only analytical expressions required for any element undergoing plane deformation.

$$\boldsymbol{A}_{TL}^{kj} = \begin{bmatrix} \vartheta_j \mathrm{diag}_n[\frac{\beta_{jn}(\Delta_{21}\Upsilon_{21}-\Delta_{22}\Upsilon_{22})}{\Sigma_2}] & \vartheta_j[\beta_{jn}\Sigma_3\Sigma_7]_{n,m} \\ \vartheta_k[\alpha_{km}\Sigma_4\Sigma_8]_{m,n} & \vartheta_k\mathrm{diag}_m[\frac{\alpha_{km}(\Delta_{11}\Upsilon_{11}-\Delta_{12}\Upsilon_{12})}{\Sigma_1}] \end{bmatrix} \quad \text{(E.1a)}$$

$$\boldsymbol{A}_{TS}^{kj} = \begin{bmatrix} \mathrm{diag}_n[\frac{\Gamma_{21}\Upsilon_{21}-\Gamma_{22}\Upsilon_{22}}{\Sigma_2}] & -\vartheta_j\vartheta_k a_2[\alpha_{km}\beta_{jn}\Sigma_7]_{n,m} \\ -\vartheta_j\vartheta_k a_2[\alpha_{km}\beta_{jn}\Sigma_8]_{m,n} & \mathrm{diag}_m[\frac{\Gamma_{11}\Upsilon_{11}-\Gamma_{12}\Upsilon_{12}}{\Sigma_1}] \end{bmatrix} \quad \text{(E.1b)}$$

$$\boldsymbol{A}_{NL}^{kj} = \begin{bmatrix} -\mathrm{diag}_n[\frac{\Delta_{21}\delta_{22}\Upsilon_{21}-\Delta_{22}\delta_{21}\Upsilon_{22}}{a_2\Sigma_2}] & [\Sigma_5\Sigma_7]_{n,m} \\ [\Sigma_5\Sigma_8]_{m,n} & -\mathrm{diag}_m[\frac{\Delta_{11}\delta_{12}\Upsilon_{11}-\Delta_{12}\delta_{11}\Upsilon_{12}}{a_2\Sigma_1}] \end{bmatrix} \quad \text{(E.1c)}$$

$$\boldsymbol{A}_{NS}^{kj} = -\begin{bmatrix} \vartheta_j\mathrm{diag}_n[\frac{\beta_{jn}(\Delta_{21}\Upsilon_{21}-\Delta_{22}\Upsilon_{22})}{\Sigma_2}] & \vartheta_k[\alpha_{km}\Sigma_4\Sigma_7]_{n,m} \\ \vartheta_j[\beta_{jn}\Sigma_3\Sigma_8]_{n,m} & \vartheta_k\mathrm{diag}_m[\frac{\alpha_{km}(\Delta_{11}\Upsilon_{11}-\Delta_{12}\Upsilon_{12})}{\Sigma_1}] \end{bmatrix}$$
$$\text{(E.1d)}$$

where $a_2 = a_0 + 1$, $\vartheta_j = (-1)^j$, $\vartheta_k = (-1)^k$ and

$$\Upsilon_{1i} = \mathcal{H}_j(t_{ikm}b)/(\mathcal{H}_k^*(t_{ikm}b)t_{ikm}), \quad \Upsilon_{2i} = \mathcal{H}_k(r_{ijn}a)/(\mathcal{H}_k^*(r_{ijn}a)r_{ijn}),$$
$$\delta_{1i} = a_1 t_{ikm}^2 + a_0\alpha_{km}^2 + \kappa, \quad \delta_{2i} = a_1 r_{ijn}^2 + a_0\beta_{jn}^2 + \kappa,$$
$$\Delta_{1i} = a_1 t_{ikm}^2 + a_0(\alpha_{km}^2 - \kappa), \quad \Delta_{2i} = a_1 r_{ijn}^2 + a_0(\beta_{jn}^2 - \kappa),$$
$$\Gamma_{1i} = a_1 t_{ikm}^2 - \alpha_{km}^2 + \kappa, \quad \Gamma_{2i} = a_1 r_{ijn}^2 - \beta_{jn}^2 + \kappa,$$
$$\Sigma_1 = a_1(t_{1km}^2 - t_{2km}^2), \quad \Sigma_2 = a_1(r_{1jn}^2 - r_{2jn}^2),$$
$$\Sigma_3 = a_1(\kappa - \beta_{jn}^2) - (3a_0 + 4)\alpha_{km}^2, \quad \Sigma_4 = a_1(\kappa - \alpha_{km}^2) - (3a_0 + 4)\beta_{jn}^2,$$
$$\Sigma_5 = 4a_2\alpha_{km}^2\beta_{jn}^2 - a_0\kappa(\alpha_{km}^2 + \beta_{jn}^2 - \kappa),$$
$$\Sigma_7 = 2(-1)^{m+n}/\left[\sqrt{\zeta_{km}\zeta_{jn}}aba_1(t_{1km}^2 + \beta_{jn}^2)(t_{2km}^2 + \beta_{jn}^2)\right],$$
$$\Sigma_8 = 2(-1)^{m+n}/\left[\sqrt{\zeta_{km}\zeta_{jn}}aba_1(r_{1jn}^2 + \alpha_{km}^2)(r_{2jn}^2 + \alpha_{km}^2)\right].$$

where the hyperbolic functions $\mathcal{H}$ and $\mathcal{H}^*$ were defined in Eq. (30). In Eq. (E.1), '$\mathrm{diag}_n[\cdot]$' represents a diagonal matrix whose diagonal terms are expressed by '$\cdot$' with the subscript n varying from 0 to ∞, whereas '$[\cdot]_{n,m}$' stands for a matrix whose entries are '$\cdot$' with n (row number) and m (column number) taking from 0 to ∞. Similarly, it is easy to understand the notations '$\mathrm{diag}_m[\cdot]$' and '$[\cdot]_{m,n}$'. Note that since the DOFs corresponding to S_{aj0}, T_{aj0} (when $j = 0$) and S_{bk0}, T_{bk0} (when

$k = 0$) in Eq. (37) have been removed, the corresponding rows and columns of the $\boldsymbol{A}^{kj}_{\bullet\bullet}$ matrices should also removed accordingly. If the notations $\boldsymbol{A}^{kj}_{\bullet\bullet}(i, :) = \emptyset$ and $\boldsymbol{A}^{kj}_{\bullet\bullet}(:, l) = \emptyset$ denote respectively the removal of the ith row and the lth column of the matrix $\boldsymbol{A}^{kj}_{\bullet\bullet}$, the following removal should be performed (assuming that $n \in [0, N - 1]$)

$$\boldsymbol{A}^{kj}_{T\bullet}(1, :) = \emptyset \text{ when } j = 0\,, \quad \boldsymbol{A}^{kj}_{T\bullet}(N + 1, :) = \emptyset \text{ when } k = 0\,, \qquad \text{(E.2a)}$$

$$\boldsymbol{A}^{kj}_{\bullet S}(:, 1) = \emptyset \text{ when } j = 0\,, \quad \boldsymbol{A}^{kj}_{\bullet S}(:, N + 1) = \emptyset \text{ when } k = 0\,, \qquad \text{(E.2b)}$$

where the subscript '$\bullet$' in Eq. (E.2a) stands for either L or S; the '$\bullet$' in Eq. (E.2b) represents either T or N.

In Eq. (E.1), the notation $(\cdot)^{kj}$ with kj taking the values '00','01','10' and '11', implies that these definitions are for all of the four symmetric/antisymmetric components. It is easily seem from Eq. (E.1) that $\boldsymbol{A}^{kj}_{TS} = \boldsymbol{A}^{kj}_{TS}{}^T$ and $\boldsymbol{A}^{kj}_{NL} = \boldsymbol{A}^{kj}_{NL}{}^T$ are symmetric matrices, while $\boldsymbol{A}^{kj}_{TL} = -\boldsymbol{A}^{kj}_{NS}{}^T$. (This *symplectic* property [40] is similar to the SDS formulation of the transverse vibration [35].)

Acknowledgements

References

[1] A. W. Leissa, The free vibration of rectangular plates, Journal of Sound and Vibration 31 (3) (1973) 257–293. `doi:10.1016/S0022-460X(73)80371-2`.

[2] A. N. Bercin, An assessment of the effects of in-plane vibrations on the energy flow between coupled plates, Journal of Sound and Vibration 191 (5) (1996) 661–680. `doi:10.1006/jsvi.1996.0149`.

[3] R. H. Lyon, In-plane Contribution to Structural Noise Transmission, Noise Control Engineering Journal 26 (1) (1986) 22–27.

[4] R. S. Langley, A. N. Bercin, Wave Intensity Analysis of High Frequency Vibrations, Philosophical Transactions of the Royal Society A: Mathematical, Physical and Engineering Sciences 346 (1681) (1994) 489–499. `doi:10.1098/rsta.1994.0031`.

[5] G. Tsiatas, G. Gazetas, Plane-strain and shear-beam free vibration of earth dams, International Journal of Soil Dynamics and Earthquake Engineering 1 (4) (1982) 150–160. `doi:10.1016/0261-7277(82)90018-3`.

[6] D. Nardini, C. A. Brebbia, A new approach to free vibration analysis using boundary elements, Applied Mathematical Modelling 7 (3) (1983) 157–162. `doi:10.1016/0307-904X(83)90003-3`.

[7] D. C. Gazis, Exact analysis of the plane-strain vibration of thick-walled hollow cylinders, The Journal of the Acoustical Society of America 30 (8) (1958) 563–568.

[8] N. Ahmed, Axisymmetric Plane-Strain Vibrations of a Thick-Layered Orthotropic Cylindrical Shell, The Journal of the Acoustical Society of America 40 (6) (1966) 1509–1516. `doi:http://dx.doi.org/10.1121/1.1910256`.

[9] H. J. Ding, H. M. Wang, P. F. Hou, The transient responses of piezoelectric hollow cylinders for axisymmetric plane strain problems, International Journal of Solids and Structures 40 (1) (2003) 105–123. `doi:10.1016/S0020-7683(02)00525-5`.

[10] H. M. Wang, H. J. Ding, Y. M. Chen, Dynamic solution of a multilayered orthotropic piezoelectric hollow cylinder for axisymmetric plane strain problems, International Journal of Solids and Structures 42 (1) (2005) 85–102. `doi:10.1016/j.ijsolstr.2004.06.059`.

[11] J. Achenbach, Wave Propagation in Elastic Solids, Elsevier, Oxford, 1973.

[12] P. Cawley, D. N. Alleyne, The use of Lamb waves for the long range inspection of large structures, Ultrasonics 34 (2-5) (1996) 287–290. `doi:10.1016/0041-624X(96)00024-8`.

[13] J. J. Ditri, Some results on the scattering of guided elastic SH waves from material and geometric waveguide discontinuities, J. Acoust. Soc. Am. 100 (5) (1996) 3078–3087. `doi:10.1121/1.417119`.

[14] M. M. Sigalas, E. N. Economou, Elastic waves in plates with periodically placed inclusions, Journal of Applied Physics 75 (6) (1994) 2845–2850. `doi:10.1063/1.356177`.

[15] S. B. Dong, R. B. Nelson, On Natural Vibrations and Waves in Laminated Orthotropic Plates, Journal of Applied Mechanics 39 (3) (1972) 739. `doi:10.1115/1.3422782`.

[16] S. B. Dong, D. B. Goetschel, Edge effects in laminated composite plates, Journal of Applied Mechanics 49 (1982) 129–135.

[17] Lord Rayleigh, The theory of sound. Volume I, Macmilllan and Co., London, 1877.

[18] D. J. Gorman, Accurate analytical type solutions for the free in-plane vibration of clamped and simply supported rectangular plates, Journal of Sound and Vibration 276 (1-2) (2004) 311–333. `doi:10.1016/j.jsv.2003.07.037`.

[19] Y. F. Xing, B. Liu, Exact solutions for free in-plane vibrations of rectangular plates, International Journal of Mechanical Sciences 51 (2009) 246–255. `doi:10.1016/j.ijmecsci.2008.12.009`.

[20] B. Liu, Y. F. Xing, Exact solutions for free in-plane vibrations of rectangular plates, Acta Mechanica Solida Sinica 24 (6) (2011) 556–567. `doi:10.1016/S0894-9166(11)60055-4`.

[21] B. Liu, Y. F. Xing, Comprehensive exact solutions for free in-plane vibrations of orthotropic rectangular plates, European Journal of Mechanics, A/Solids 30 (3) (2011) 383–395. `doi:10.1016/j.euromechsol.2011.01.003`.

[22] W. H. Wittrick, F. W. Williams, Buckling and vibration of anisotropic or isotropic plate assemblies under combined loadings, International Journal of Mechanical Sciences 16 (4) (1974) 209–239. `doi:10.1016/0020-7403(74)90069-1`.

[23] N. S. Bardell, R. S. Langley, J. M. Dunsdon, On the free in-plane vibration of isotropic rectangular plates, Journal of Sound and Vibration 191 (3) (1996) 459–467. `doi:10.1006/jsvi.1996.0134`.

[24] A. N. Bercin, R. S. Langley, Application of the dynamic stiffness technique to the in-plane vibrations of plate structures, Computers & structures 59 (5) (1996) 869–875.

[25] M. Boscolo, J. R. Banerjee, Dynamic stiffness method for exact inplane free vibration analysis of plates and plate assemblies, Journal of Sound and Vibration 330 (12) (2011) 2928–2936. `doi:10.1016/j.jsv.2010.12.022`.

[26] L. Dozio, Free in-plane vibration analysis of rectangular plates with arbitrary elastic boundaries, Mechanics Research Communications 37 (7) (2010) 627–635. `doi:10.1016/j.mechrescom.2010.09.003`.

[27] N. H. Farag, J. Pan, Free and forced in-plane vibration of rectangular plates, The Journal of the Acoustical Society of America 103 (1) (1998) 408. `doi: 10.1121/1.421120`.

[28] N. H. Farag, J. Pan, Modal characteristics of in-plane vibration of rectangular plates, Acoustical Society of America 105 (6) (1999) 3295–3310. `doi: 10.1121/1.424658`.

[29] G. Wang, N. M. Wereley, Free In-Plane Vibration of Rectangular Plates, AIAA Journal 40 (5) (2002) 953–959. `doi:10.2514/2.1732`.

[30] D. J. Gorman, Free in-plane vibration analysis of rectangular plates by the method of superposition, Journal of Sound and Vibration 272 (3-5) (2004) 831–851. `doi:10.1016/S0022-460X(03)00421-8`.

[31] M. Nefovska-Danilovic, M. Petronijevic, In-plane free vibration and response analysis of isotropic rectangular plates using the dynamic stiffness method, Computers & Structures 152 (2015) 82–95. `doi:10.1016/j. compstruc.2015.02.001`.

[32] J. Du, W. L. Li, G. Jin, T. Yang, Z. Liu, An analytical method for the in-plane vibration analysis of rectangular plates with elastically restrained edges, Journal of Sound and Vibration 306 (2007) 908–927. `doi:10. 1016/j.jsv.2007.06.011`.

[33] J. Du, Z. Liu, W. L. Li, X. Zhang, Free In-Plane Vibration Analysis of Rectangular Plates With Elastically Point-Supported Edges, Journal of Vibration and Acoustics 132 (3) (2010) 031002. `doi:10.1115/1.4000777`.

[34] S. O. Papkov, A new method for analytical solution of inplane free vibration of rectangular orthotropic plates based on the analysis of infinite systems, Journal of Sound and Vibration (2016) 1–18`doi:10.1016/j. jsv.2016.01.025`.

[35] X. Liu, J. R. Banerjee, Free vibration analysis for plates with arbitrary boundary conditions using a novel spectral-dynamic stiffness method, Computers & Structures 164 (2016) 108–126. `doi:10.1016/j. compstruc.2015.11.005`.

[36] X. Liu, J. R. Banerjee, An exact spectral-dynamic stiffness method for free flexural vibration analysis of orthotropic composite plate assemblies - Part I: Theory, Composite Structures 132 (2015) 1274–1287. `doi:10.1016/j. compstruct.2015.07.020`.

[37] X. Liu, J. R. Banerjee, An exact spectral-dynamic stiffness method for free flexural vibration analysis of orthotropic composite plate assemblies - Part II: Applications, Composite Structures (132) (2015) 1288–1302. `doi:10.1016/j.compstruct.2015.07.022`.

[38] A. Iserles, S. P. Nørsett, From high oscillation to rapid approximation I: Modified Fourier expansions, IMA Journal of Applied Mathematics 28 (4) (2006) 862–887. `doi:10.1093/imanum/drn006`.

[39] S. Olver, On the Convergence Rate of a Modified Fourier Series, Mathematics of Computation 78 (267) (2009) 1629–1645.

[40] W. X. Zhong, Duality System in Applied Mechanics and Optimal Control, Kluwer Academic Publishers, London, 2004.

[41] X. Liu, H. I. Kassem, J. R. Banerjee, An exact spectral dynamic stiffness theory for composite plate-like structures with arbitrary non-uniform elastic supports, mass attachments and coupling constraints, Composite Structures 142 (2016) 140–154. `doi:10.1016/j.compstruct.2016.01.074`.

[42] W. H. Wittrick, F. W. Williams, A general algorithm for computing natural frequencies of elastic structures, The Quarterly Journal of Mechanics and Applied Mathematics XXIV (3) (1971) 263–284. `doi:10.1093/qjmam/24.3.263`.

[43] D. J. Gorman, Exact solutions for the free in-plane vibration of rectangular plates with two opposite edges simply supported, Journal of Sound and Vibration 294 (1-2) (2006) 131–161. `doi:10.1016/j.jsv.2005.10.023`.

[44] R. K. Guy, Unsolved problems in number theory, 3rd Edition, Springer, New York, 2004.

[45] L. E. Monterrubio, S. Ilanko, Proof of convergence for a set of admissible functions for the RayleighRitz analysis of beams and plates and shells of rectangular planform, Computers & Structures 147 (2015) 236–243. `doi:10.1016/j.compstruc.2014.09.008`.

[46] D. J. Rixen, A. Boogaard, M. V. Van Der Seijs, G. Van Schothorst, T. Van Der Poel, Vibration source description in substructuring: A theoretical depiction, Mechanical Systems and Signal Processing 60 (2015) 498–511. `doi:10.1016/j.ymssp.2015.01.024`.